FABRICATION AND CHARACTERIZATION OF BISMUTH HALL SENSORS AT ROOM TEMPERATURE

A THESIS
SUBMITTED TO THE DEPARTMENT OF PHYSICS
AND THE INSTITUTE OF ENGINEERING AND SCIENCE
OF BILKENT UNIVERSITY
IN PARTIAL FULFILLMENT OF THE REQUIREMENTS
FOR THE DEGREE OF
MASTER OF SCIENCE

By
Gözde Bayer
September, 2003

FABRICATION AND CHARACTERIZATION OF BISMUTH HALL SENSORS AT ROOM TEMPERATURE

A THESIS

SUBMITTED TO THE DEPARTMENT OF PHYSICS

AND THE INSTITUTE OF ENGINEERING AND SCIENCE

OF BILKENT UNIVERSITY

IN PARTIAL FULFILLMENT OF THE REQUIREMENTS

FOR THE DEGREE OF

MASTER OF SCIENCE

By

Gözde Bayer

September, 2003

I certify that I have read this thesis and that in my opinion it is fully adequate, in scope and in quality, as a thesis for the degree of Master of Science.

Assoc. Prof. Dr. Ahmet Oral (Supervisor)

I certify that I have read this thesis and that in my opinion it is fully adequate, in scope and in quality, as a thesis for the degree of Master of Science.

Assoc. Prof. Dr. Recai Ellialtıoğlu

I certify that I have read this thesis and that in my opinion it is fully adequate, in scope and in quality, as a thesis for the degree of Master of Science.

Asst. Prof. Dr. Okan Tekman

Approved for the Institute of Engineering and Science

Prof.Dr. Mehmet Baray

Director of the Institute of Engineering and Science

FABRICATION AND CHARACTERIZATION OF BISMUTH HALL SENSORS AT ROOM TEMPERATURE

Gözde Bayer

M. Sc. in Physics

Supervisor: Assoc. Prof. Dr. Ahmet Oral

September, 2003

Small-scale Hall effect devices have attracted a great deal of research interest in recent years. It is well known that bulk single crystal of bismuth exhibit a large magnetoresistance effect and the recognition of this fact has stimulated a number of recent efforts to grow thin films of bismuth. Such films are useful in magnetic sensing applications.

We fabricated Hall sensors having thickness of 30 nm and 50 nm of Bismuth using photolithography. Bismuth was deposited on to the surface of GaAs by evaporation technique. The properties of these sensors were then studied: dependences of the resistivity, and Hall coefficient on layer thickness were investigated at room temperature, Hall coefficients were calculated under the effect of a magnetic field. Results were then compared with the previously obtained values.

Bismuth micro-Hall probes with dimensions as small as $\approx 0.25\ \mu m \times 0.25\ \mu m$ produced by Focused Ion Beam (FIB) milling were also presented in this study. Hall coefficient was then calculated.

Keywords: Bismuth Hall Sensors, electrical resistivity, Hall effect, Hall coefficient

ÖZET

BISMUTH HALL ALGILAYICILARININ YAPIMI VE ODA SICAKLIĞINDA KARAKTERİZASYONU

Gözde Bayer
Fizik, Yüksek Lisans
Tez Danışmanı: Doç. Dr. Ahmet Oral
Eylül, 2003

Küçük ölçekli Hall etkisi sensörleri son yıllarda yaygın olarak araştırmaların konusu olmaya başlamıştır. Kristal bizmut kümesi büyük bir manyetik-direnç etkisi göstermektedir ve bu özelliğinden dolayı Bizmutun ince filmler halinde yapılması üzerine çalışılmaya başlanmıştır. Bu tür yapılar manyetik algılama uygulamalarında fayda sağlamaktadır.

Bu çalışmada fotolithografi tekniği kullanılarak Bizmut kalınlığı 30 ve 50 nm olan Hall etkisi aygıtları yapılmıştır. Bizmut GaAs yarıiletkeni üzerine buharlaştırma ile eklenmiştir. Daha sonra bu Hall aygıtlarının özellikleri incelenmeye başlanmıştır : dirençlilik ve Hall katsayısı farklı kalınlık için oda sıcaklığında ölçülmüştür, Hall etkisi manyetik alan etkisi altında incelenmis, sonuçlar daha önce literatürde bulunanlarla karşılaştırılmıştır.

Bu çalışmada, Odaklanmış Ion Demeti (OID) yöntemi ile yapılan 0.25 μm × 0.25 μm boyutlarındaki Bizmut mikro-Hall sensörleri ve bunlar için hesaplanan Hall katsayısı da verilmektedir.

Anahtar Kelimeler : Bizmut Hall sensörleri, elektriksel dirençlilik, Hall etkisi, Hall katsayısı

ACKKNOWLEDGEMENTS

I would like to express my deepest gratitude to my supervisor Assoc. Prof. Ahmet Oral for his invaluable supervision, helpful suggestion and comments throughout the course of this investigation.

I would like to thank especially to Münir Dede for allocating his time to teach me about some experimental details at many stages of this work.

I owe special thanks to Assoc.Prof. Mehmet Parlak for his help at the Bismuth evoporation step at Middle East Technical University.

I would like to thank also Prof. Adarsh Sandhu who participated in the calculation of the Hall coefficient of the Bi-micro Hall probes fabricated by FIB milling.

I wish to thank to Serdar Özdemir and Merhdad Atabak for their help and remarks.

I also wish to thank to Ergün Karaman for the technical help.

Finally my thanks are due A.Murat Güler who cheered me up especially at the last stages of this work.

Contents

List of Figures

List of Tables

Chapter 1

Introduction

Bismuth is a semimetal with unusual electronic properties related to its highly anisotropic Fermi surface, small carrier effective masses (0.00651 m_o) and long carrier mean free path. Crystalline bismuth has a mean free path of ~250 nm at 300 K. It has a band overlap of about 38 meV at 0 K. Bismuth has a high mobility $\mu=3.5 \times 10^4$ $cm^2/V.s.$ with $n_e \approx 10^{18}$ cm^{-3}. Bi is a poor thermoelectric because of its low Seebeck coefficient, contributions from both electrons and holes approximately cancel. In bulk bismuth, the three conduction band minima at the L points lie nearly 40 meV lower than the single crystal valence band maximum at the T point (Figure 1.1).

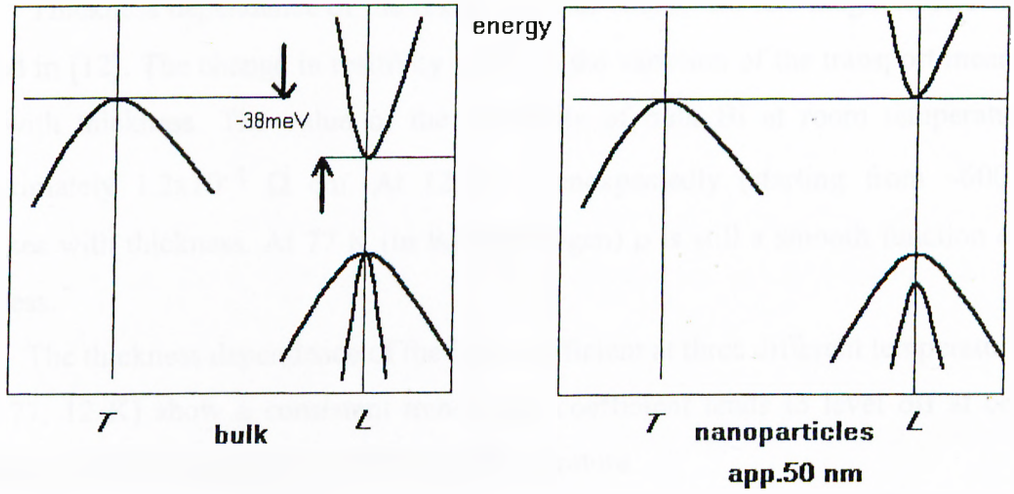

Figure 1.1. Bismuth Band Structure

As a result of these properties, finite size effects are easily observed in thin films, nanowires and lithographically pattern crystals.

The carrier mean free path may be as large as 1 mm at 4.2 K, many orders of magnitude larger than for most metals, giving rise to very large magnetoresistance effect [1]. Recently bismuth has attracted much attention for applications that involve field and current sensing due to this property. Because of these properties, along with a large Fermi wavelength of 400 A°, bismuth has frequently been used for quantum confinement studies of quantum well and quantum wire geometries [2].

In a 1965 magnetotransport study of bismuth thin films by Ogrin [3] when the film thickness was varied, both the resistivity and the Hall coefficient displayed oscillations. The amplitude of the oscillations in the resistivity increases with increasing thickness. Moreover, the oscillations at 77 K are almost as pronounced as those at 4.2 K. Arguments for and against the existence of a semiconducting phase have focused on the presence or absence of sudden changes in the resistivity, Hall coefficient and magnetoresistance as functions of layer thickness [4]. In the work of [4] the resistivity and Hall coefficient were measured as a function of magnetic field ($0 \leq B \leq 7$ T) and temperature ($4.2 < T < 300$ K) by the van der Pauw technique.

Thickness dependence of the resistivity, hall coefficient and magnetoresistance is studied in [12]. The change in resitivity is due to the variation of the transport mean-free path with thickness. The value of the resistivity of bulk Bi at room temperature is approximately 1.2×10^{-4} Ω cm. At 12 K, ρ unexpectedly (starting from ~600 °A) increases with thickness. At 77 K (in liquid nitrogen) ρ is still a smooth function of the thickness.

The thickness dependence of the Hall coefficient at three different temperatures (360, 77, 12 K) show a consistent trend: Hall coefficient tends to level off at certain thickness, which decreases with increasing temperature.

[13] demonstrated that, due to band bending related to impurity states either at the surface or at the interface with the substrate, the low-temperature electron concentrations in a series of films varied as

$$n_s \sim n_i + n_s/d ,$$

where n_i is the bulk intrinsic concentration resulting from the energy overlap of the conduction and valence bands, and n_s is the sheet density associated with surface states.

Dependences of mobilities for the electrons and holes on temperature were also studied in [13]. While both μ_n and μ_p could be determined at all temperatures in the 5000 angstrom (500nm) film, data for the thinner samples showed no evidence for electrons in the low T limit (Figure 1.2)

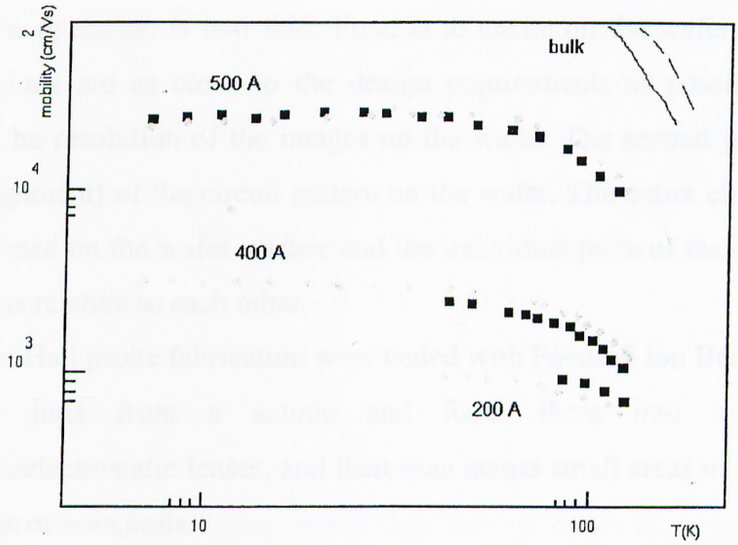

Fig. 1.2. Mobilites for electrons (dark points) and holes (lighter points) vs. temperature in three of the films. The curves represent bulk dependences for electrons (dashed) and holes (solid) [13].

Some authors [14] and [15] have also studied the possibility of using quantum confinement to convert the material into a semiconductor.

Chapter 2

Fabrication of Bismuth Hall Sensors

2.1 Introduction

Photolithography is one of the most critical operations in semiconductor processing. The goal of the operation is two fold. First, is to create on the wafer surface a pattern whose dimensions are as close to the design requirements as possible. This goal is referred to as the resolution of the images on the wafer. The second goal is the correct placement (alignment) of the circuit pattern on the wafer. The entire circuit pattern must be correctly placed on the wafer surface and the individual parts of the circuit must be in correct positions relative to each other.

Some of the Hall probe fabrication were ended with Focused Ion Beam milling which uses Gallium ions from a source and focus them into a beam through electromagnetic/electrostatic lenses, and then scan across small areas of the sample using deflection plates or scan coils.

2.2. Overview of the Optical Lithography Process

Photolithography is a multi-step pattern transfer process. There are some basic steps involved in the process namely, cleaning, coating, pre-bake, alignment, exposure, development, post-bake, processing and inspection. Each procedure will be discussed briefly in the following sections.

2.2.1. Cleaning

Semiconductor devices are very vulnerable to many types of contaminants. This is the reason why clean wafers are essential at all stages of the fabrication process. Wafer surfaces can, in general, have four types of contamination: particulates, organic residues, inorganic residues and unwanted oxide layers. The simplest particulate removal process is to blow off the wafer surface using a high-pressure nitrogen from a handheld gun. The organic residues on the other hand can be removed in solvents baths such as acetone or TCE. A typical process may be one bath of TCE followed by an isopropyl alcohol rinse, followed by an acetone rinse. Each of the succeeding rinse dissolves the previous solvent.

Inorganic residues are cleaned from the wafers by for example hydrogen peroxide added to sulfuric acid. The chemicals used in cleaning the wafers can also be contaminants if left on the surface. Therefore every cleaning process or sequence is followed by a rinse in de-ionized water. The water also serves to end the etching action of the oxide in the removal steps.

2.2.2. Coating with Photoresist

Coating is a step to apply photoresist onto the wafer. A uniformly coated wafer usually has higher chances of getting the desired pattern transferred in the later processes. This section will outline the steps of spin coating with AZ 5214 photoresist. Some properties of the photoresist are listed in Table 2.1.

Spin speed (rpm)	3000	4000	5000	6000
Thickness (μm)	1.62	1.40	1.25	1.14
Pre-bake	110° C, 50 sec hotplate			
Exposure	Broadband and monochromatic h and i line			
Reversal bake	120° C, 2 min hotplate (most critical step)			
Development	AZ 351B, 1:4 or AZ 726 (puddle)			
Post-bake	120° C, 50s hotplate (optional)			
Removal	AZ 100 Remover			

Table 2.1. Processing guidelines for AZ 5214 Photoresist

Initial Stage

1. Make sure that the wafer is clean and dry. Visible dust on the wafer can be removed by gently blowing the wafer using nitrogen gas.
2. Turn on the vacuum supply and make sure that the vacuum supply on the spinner is functioning properly.
3. Input the correct 'recipe' into the spinner through the control buttons.

The purpose of the photoresist application step is the establishment of a thin, uniform, defect-free film of photoresist on the wafer surface. A typical resist layer varies from 0.5 to 1.5 μm in thickness and has to have a uniformity of plus or minus 0.01 μm (100 A°). The final thickness of the film is established as the result of the resist viscosity, the spin speed, the surface tension and the drying characteristics of the resist. The relation between the spin speed and the resist thickness is shown in Fig. 2.1.

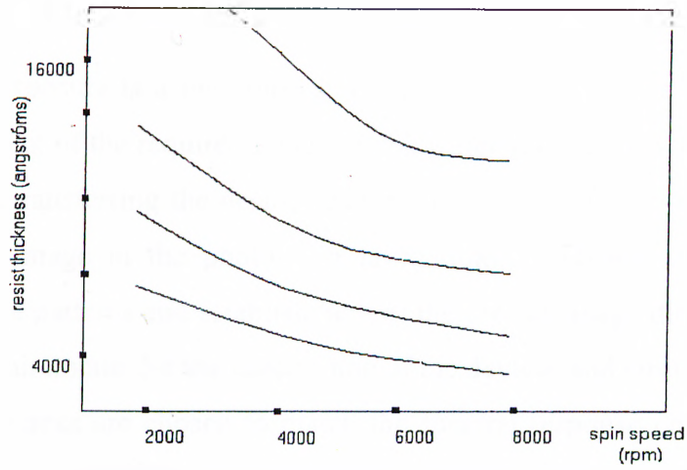

Fig. 2.1.The relation between the spin speed and the resist thickness

Final Stage

1. The spinner will stop automatically when spin coating is completed.
2. Remove the wafer from the spinner chuck and check the pattern of the coated wafer.
3. Make sure that the photoresist has been uniformly coated. If striations and streaks are observed, the spin coating is not successful. Acetone can be used to strip off the resist.

2.2.3. Prebake (Softbake)

Prebake step is a heating operation with the purpose of evaporating a portion of the solvents in the photoresist. The solvents are evaporated for two reasons. They can absorb exposing radiation, thus interfere with the proper chemical change in the photosensitive polymers. The second problem is with the resist adhesion. The complete drying (evaporation of the solvent) is necessary for good adhesion.

2.2.4. Alignment and Exposure

Alignment and exposure is a two-purpose photo-masking step. The first part is the positioning or alignment of the required image on the wafer surface. It will determine the successfulness of the transferring the desired patterns onto the wafer. The second part is the encoding of the image in the photoresist layer from a radiation source. Correct alignment of the image patterns and establishment of the precise image dimensions in the resist are absolute requirements for the functioning of the devices and circuits.

Exposure light sources are chosen to match the spectral response characteristics of the resist and the feature size of the images. Most optical aligner systems (Fig 2.2.) use a high-pressure mercury lamp.

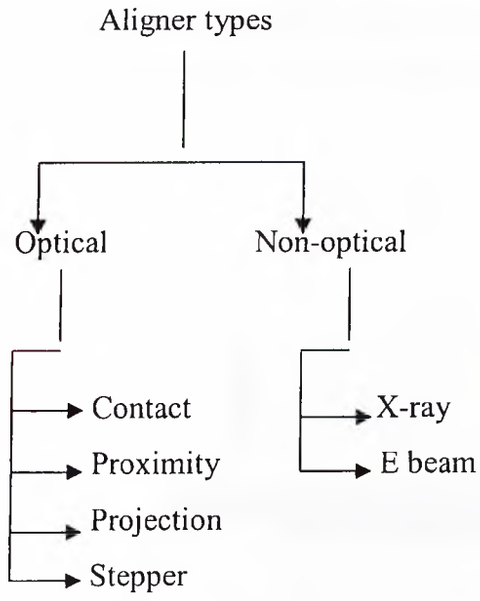

Fig. 2.2. Table of aligner types

The energy from the mercury comes out in bundles of waves grouped in ranges. Some resists are designed to react the entire range of the wavelengths and some to specific wavelengths. Other resists are designed to respond to the specific high-energy peaks of a mercury lamp. The three peaks are at the 365, 405 and 436 nm. They are

referred to I, H and G lines, respectively. AZ 5214 photoresist has spectral absorption peak at about 360 nm, so it is ideally matched for mercury i-line photolithography.

Until the mid 1970s, the contact aligner was the workhorse aligner of the semiconductor industry. The alignment part of the system uses a full-wafer-size photomask positioned over a vacuum wafer chuck. The chuck is moved left, right and can be rotated by manual controls until the wafer is aligned to the mask pattern (Fig 2.3.).

Once the mask and the wafer are aligned properly, the aligner is put into the exposure mode. First the wafer chuck moves up on a piston. Pushing the mask into intimate contact with the mask. Once the contact is established, a mirror is activated which directs the ultraviolet rays coming from a reflection and lens system through the mask and into the photoresist. A properly adjusted exposure ray is referred to as a *collimated* light.

In the contact mode, any particulate contamination will damage the soft resist layer, the mask or both. Dirt between the mask and wafer will cause resolution problems in the immediate area of piece of dirt, due to the forced local separation of the mask and wafer.

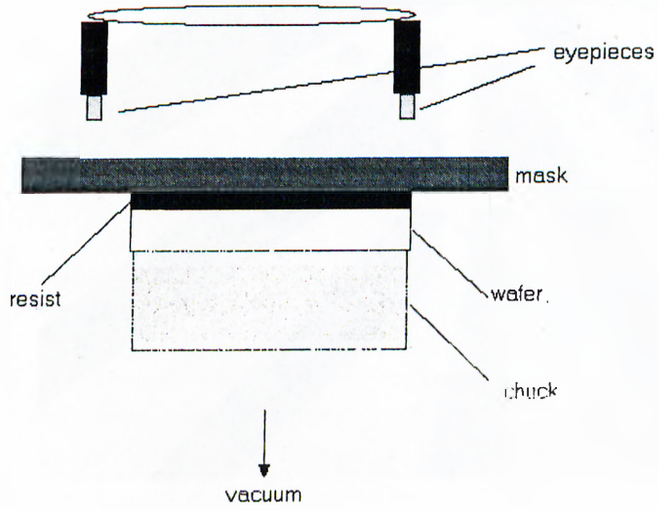

Fig 2.3. Contact aligner system – contact mode

Mask alignment and exposure steps were carried out by Karl-Suss MJB 3 Mask Aligner. Following alignment, the photoresist is exposed through the mask with high-intensity UV light from a mercury lamp of power 350 W (with λ=320 nm). The transferred pattern onto GaAs is shown in Figure 2.4 below.

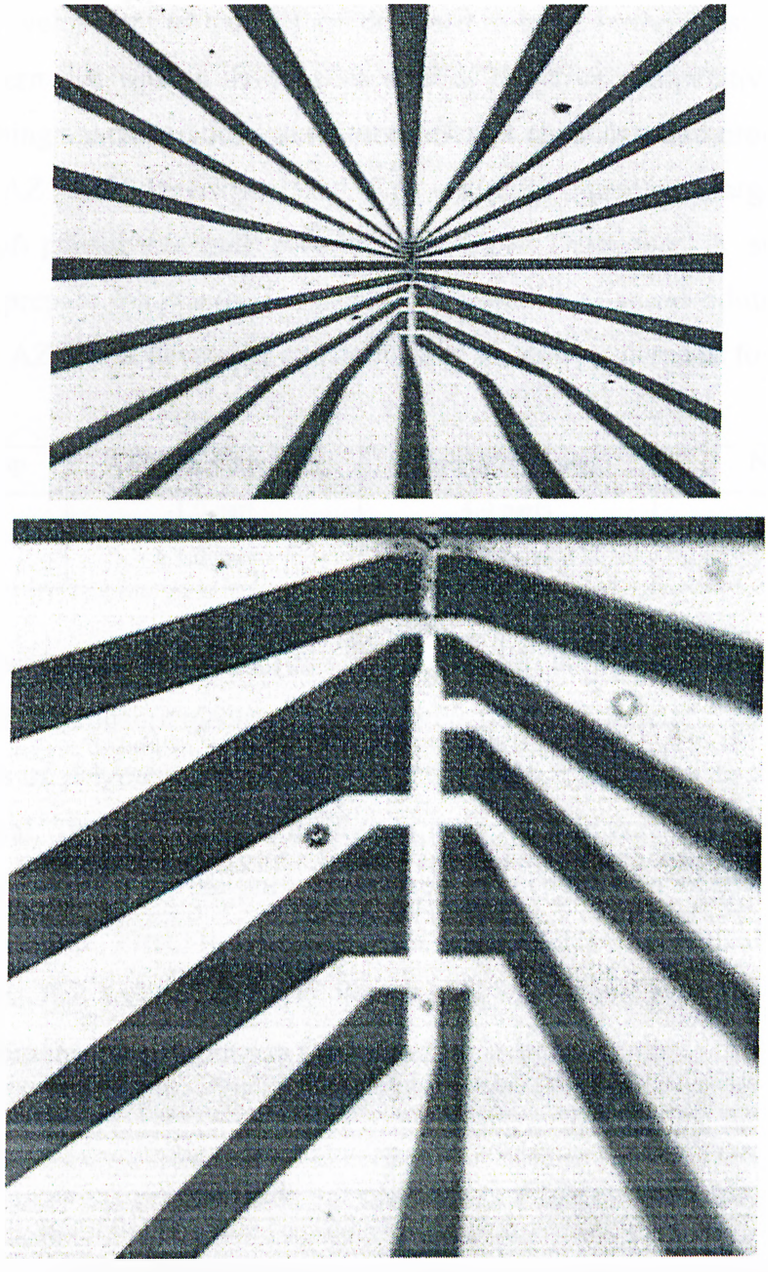

Figure 2.4. Hall Probe definition mask —— 10 μm

2.2.5. Development

After the wafer completes the alignment and exposure step, the device or circuit pattern is coded in the photoresist as regions of exposed and unexposed resist. The pattern is 'developed' in the resist by the chemical dissolution of the un-polymerized resist regions. Development techniques are designed to leave in the resist layer an exact copy of the pattern that was on the mask or reticle. Negative and positive resists have different developing characteristics and require different chemicals and processes. In this study we used AZ 400K Developer that is an odorless, aqueous, inorganic, alkaline solution, free of phosphates and sodium. AZ 400K Developer is supplied as a concentrate. To prepare the standard high resolution and high-speed dilutions from the concentrate, mix AZ 400 K developer and de-ionized water by volume as follows:

Developer Make-up	AZ 400K Developer	De-ionized water	Normality
High Contrast	1.0 part	4.0 parts	0.28 N
High Speed	1.0 part	3.0 parts	0.35 N

The successful development of the image coded in the resist is dependent on the nature of the resist's exposure mechanisms. Negative resist, upon exposure to light, goes through a process of polymerization that renders the resist resistant to dissolution in the developer chemical. The dissolving rate between the two regions is high enough so that little of the resist is lost from the polymerized regions. The action of the rinse, on the other hand, is twofold. First, it rapidly dilutes the developer chemical to stop the developing action. The second action of the rinse is to remove partially polymerized pieces of resist from the open regions in the resist film.

2.2.6. Hard Bake

Hard bake is the second heat treatment operation in the masking process. Its purpose is essentially the same as the soft bake step: the evaporation of solvents to harden the

resist. For hard bake, however, the goal is exclusively to achieve good adhesion of the resist to the wafer surface.

2.2.7. Contact Metalization

The metal contact is formed on the sample for electrical connections. This process is based on heating the source material to the point of vaporization in high vacuum atmosphere and then depositing onto sample surface. The chamber pressure of the order of 10^{-6} mbar is achieved in Leybold L560 Box Coater before the process started. The samples are initially mounted on a holder with their front surface facing the material holder (boat) below. Materials, such as gold and titanium, are then placed into respective boats and evaporated in order to deposit a thin film covering the surface of the wafer.

Partially gold is used for the upper metal because its ductile, oxide free nature allows easy bonding. The reason for using Titanium which shows good stable thermal properties on GaAs was to improve contact quality by providing better adhesion.

The features desired in a metalization step are contact uniformity, controllable deposition of thin layers, reproducibility and reliability. However, one problem that sometimes arise in this step was the easy lift-off of coated layer from the surface.

Ohmic Contact metalization was followed by Hall probe definition step by evaporating Bismuth on pattern on Gallium Arsenic.

2.2.8. Bismuth Evaporation

Deposition of bismuth on to GaAs substrate was performed at Middle East Technical University (Ankara) by Nanotech Thermal Coating System. The system composes of vacuum (diffusion) pump, electrical leads for heating source (Bi), shutter and sample holder. A thin glass sheet was used to calibrate the thickness of Bismuth layer. At approximately 4.5 minutes, a thickness of 30 nm and at 6.5 minutes, 50 nm thick Bismuth film was achieved. The dependence of thickness on deposition time was not so linear.

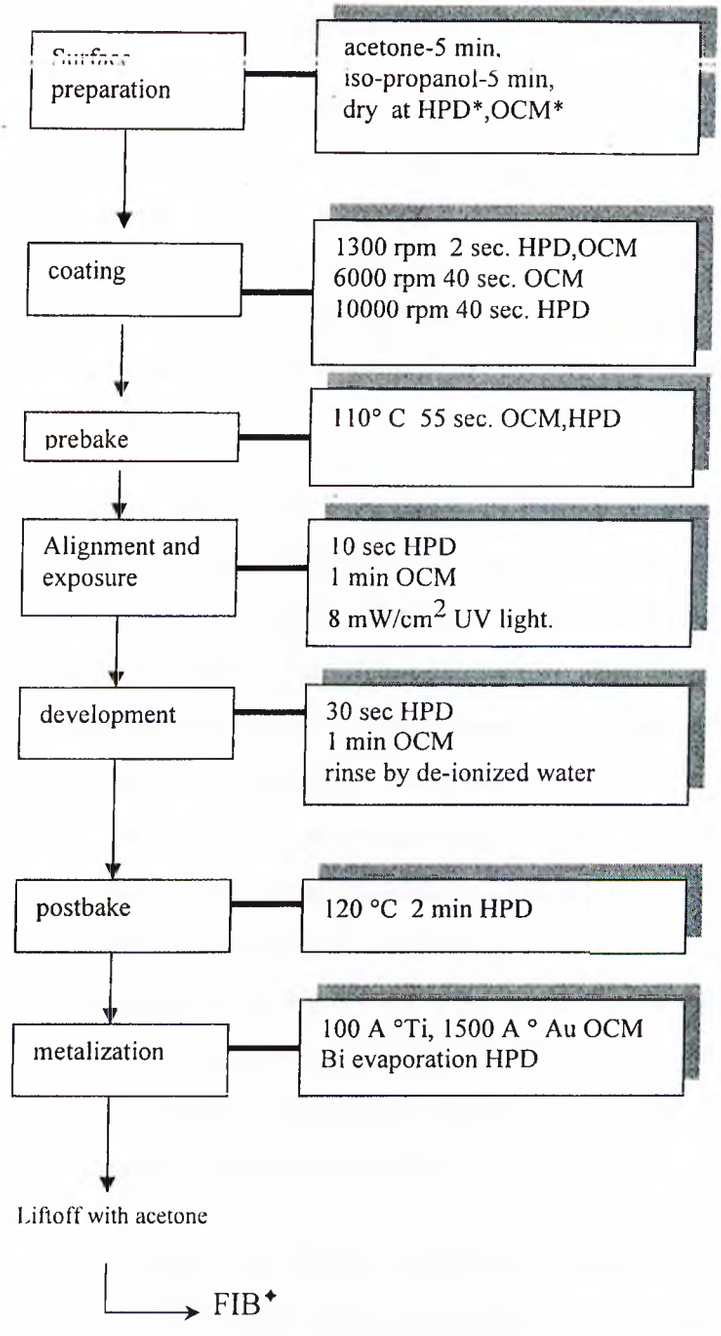

Fig. 2.5. Photolithography Quick Reference

- * HPD: Hall Probe Definition, OCM: Ohmic Contact Metalization
- ✦ Skips the HPD step

2.3. Focused Ion Beam Milling

The Focused Ion Beam (FIB) technology is used for investigation in materials research or microelectronics, especially for high contrast imaging of thin film microstructure using the channeling effect, cross section preparation, failure analysis, microstructuring or thin film device modification. Using a focused gallium ion beam, it can precisely remove or deposit material at the sample surface on a submicron scale as well as image the sample surface producing high quality contrast images with high magnifications.

In the focused ion beam system (FIB), a highly focused ion beam is aimed at a target area on the sample. As the beam scans the surface of the sample, a highly magnified image is created, allowing the system operator to clearly view the samples microscopic features. The FIB offers the ability to perform nanopatterning and micromachining respectively, and by instructing the machine to add or remove pertinent features, operator can design and prototype a new micro or nanostructure, modify integrated circuits and cross section specific features to allow failure analysis even in the 3rd dimension. In a maskless process the FIB allows the fabrication of ultrafine structures by direct deposition of metal (tungsten, gold, iron) or insulator schemes (silicondioxide) with a minimum feature size down to 30 nm and a nesting tolerance of 10 nm. Composite materials can be selectively etched in reactive gas atmospheres achieving aspect ratios up to 30 with a minimum feature size below 25 nm. The ion beam itself could be used to perform spatially confined Ga-doping.

A focused ion beam workstation operates similar to a scanning electron microscope (SEM) in that both instruments take charged particles from a source, focus them into a beam through electromagnetic/electrostatic lenses, and then scan across small areas of the sample using deflection plates or scan coils. Both instruments are used for high resolution imaging by collecting the secondary electron emission produced by the beam's interaction with the sample surface. Contrast is formed by raised areas of the sample (hills) producing more secondary electrons than depressed areas (valleys). Within reasonable beam currents an electron beam is nondestructive, but since gallium ions are

orders of magnitude more massive than electrons, an FIB's ion beam mills the sample surface as it images it. Unfortunately, an ion beam will not etch through unlimited thickness of material. This limitation depends on sample composition, mill area, beam parameters and so on. But by injecting a reactive gas into the mill process, the aspect ratio of the ion beam's cutting depth can be dramatically altered.

A focused ion beam can also be used to deposit material. Some organic and organometallic compounds have high enough vapor pressures that they may be injected as a gas into the vacuum chamber where they are adsorbed onto the sample surface. When this precursor molecule is struck by either the incident gallium ion beam or by secondary emission products (phonons), the chemical bonds holding it together break, releasing the carbon atoms into the FIB's vacuum chamber. The heavier platinum atom is then deposited as an electrical conductor onto the sample surface. The deposition process or other materials is similar. For example, silicon rich insulating films can be deposited using organosilane precursors.

Figure 2.6.1 is a scanning electron microscope image before the Hall probe was milled. Figure 2.6.2 is the view of a Bi micro-Hall probe produced by FIB milling with scanning gallium ions focused over the cross region. The scanning ion microscope mode of the FIB system was used for monitoring the device structure before and after milling. FIB milling was done at Trinity College in Ireland.

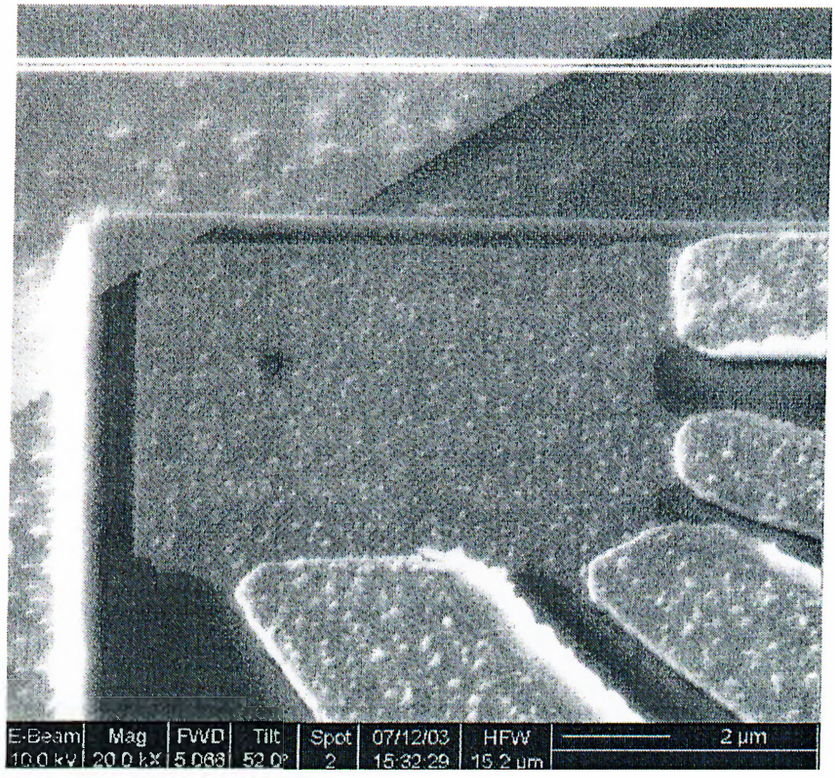

Figure 2.6.1. SEM image before the Bi hall probe was milled.

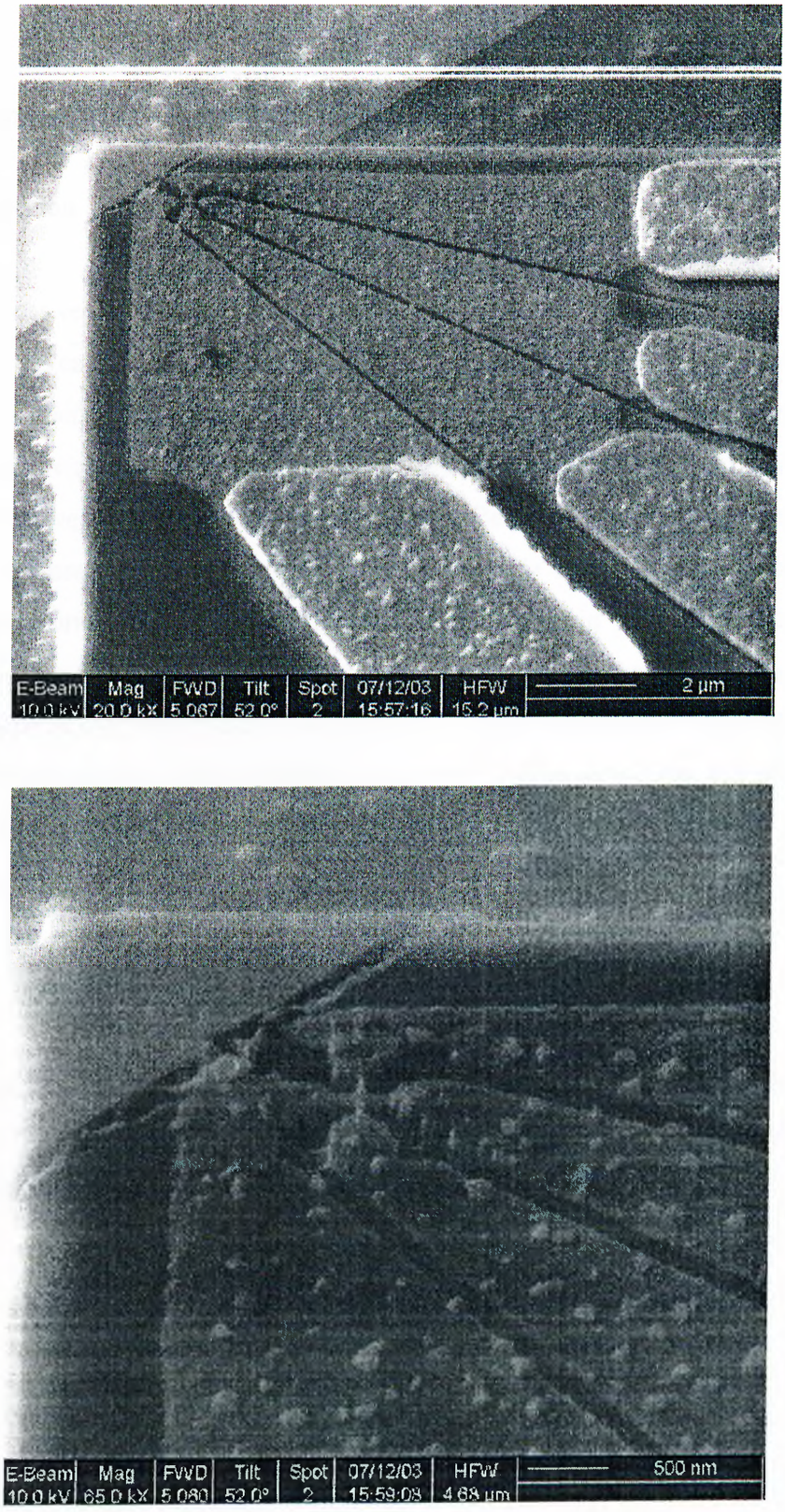

Figure 2.6.2. SEM image after the Bi hall probe was milled.

Chapter 3

Measurement with Bismuth Hall Sensors

3.1. Introduction

The objective of this section is to describe the Hall measurement technique for determining the carrier density and mobility in semiconductor materials. The importance of the Hall effect is underscored by the need to determine accurately carrier density, electrical resistivity, and the mobility of the carriers in semiconductors. The Hall effect provides a relatively simple method for doing this. Because of its simplicity and low cost, it is an indispensable characterization technique in the semiconductor industry and in research laboratories. The history of the Hall effect begins in 1879 when Edwin H. Hall discovered that a small transverse voltage appeared across a current-carrying thin metal strip in an applied magnetic field. Until that time, measurements provided only the carrier density-mobility product. Development of the Hall effect technique has since led to a mature and practical tool for testing the electrical properties and quality of almost all of the semiconductor materials.

3.2. Theory of the Hall Effect

Let us begin by considering the motion of charge carriers, each of charge q, in a conductor of thickness b and width as shown in Figure 3.1. This element is referred to as the Hall element.

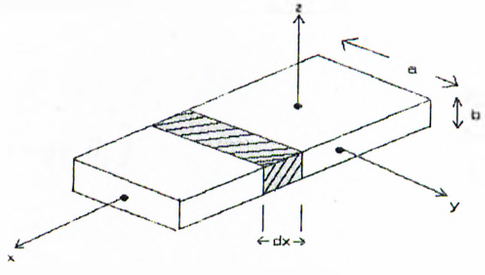

Figure 3.1. The Hall Element

If there are N charge carriers per unit volume, each small element of length dx contains a charge

$$dQ = Nqabdx \tag{3.1}$$

associated with the carriers. A current is made to flow in the +x direction if a battery is connected to the ends of the strip as shown. The carriers are accelerated but, because of the collisions with the conductor, they attain an average velocity V_X called the drift velocity. In a time *dt* the carriers move and average distance ds = V_X *dt*. Hence a charge

$$ds = Nqab\ V_X\ dt \tag{3.2}$$

passes out of each volume element into the next during a time interval *dt*. This just describes a current I_C =dQ/*dt* which we will call the control current. We can then write

$$v_X = \frac{Ic}{Nqab} \tag{3.3}$$

If we now turn on a magnetic field $\vec{B} = B_z \hat{k}$ as shown in Figure 3.2, the drifting carriers experience an additional force

$$\vec{F} = q(\vec{v} \times \vec{B}) = -qv_x B_z \hat{j} \tag{3.4}$$

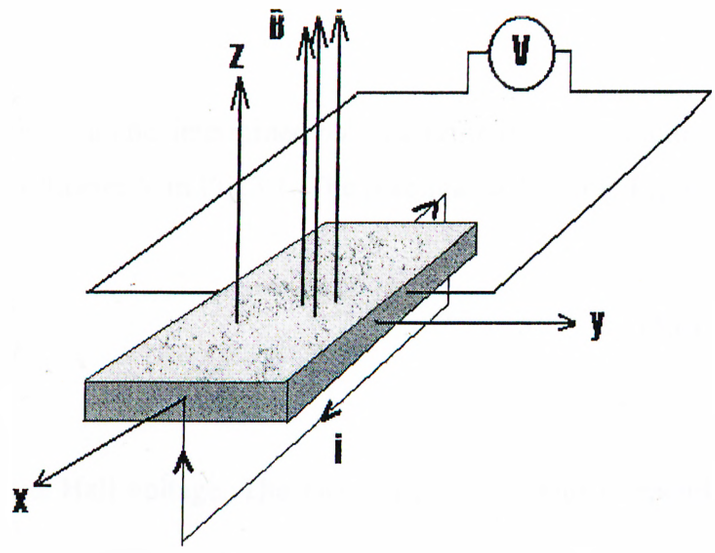

Figure 3.2. Electrical Connections to the Hall Element

As a result the charge carriers move to the –y edge of the conductor producing a net charge density +s and leaving a deficiency of carriers on the +y edge resulting in a charge density there of –s. This gives rise to an electric field in the +y direction E_y. This field exerts a force q E_yj on the carriers which opposes the magnetic force of Eq.(3.4). Carriers continue to flow toward the –y edge until the electric force and the magnetic force balance, that is, until

$$qE_y \hat{j} - qV_x B_z \hat{j} = 0$$

Substituting the value of v_x from Eq. (3.3) we find

$$E_y = \frac{I_c B_z}{Nqab} \tag{3.5}$$

This equilibrium field can be determined by measuring the potential difference across the sample using the voltmeter V in Fig.3.1. The potential difference, V_H, is

$$V_H = -\frac{I_c B_z}{Nqb} \tag{3.6}$$

V_H is known as the Hall voltage. The factor $R_H = \frac{1}{Nq}$, which depends entirely on the material of which the Hall element is made, is called the Hall coefficient. We can rearrange Eqn. (3.6) into the form

$$B_z = -\left(\frac{b}{R_H}\right)\frac{V_H}{I_c} \tag{3.7}$$

Table 3.1 gives typical Hall coefficients for various materials at room temperature [6,7,8]. The reason the Hall coefficient is negative for some materials is that the charge carriers in these materials are electrons for which q = - | e |. In other cases the carriers are "holes" whose charge is positive.

Material	R_H(m^3/coul)
Cu	-5.3×10^{-11}
Na	-21×10^{-11}
Cr	35×10^{-11}
Bi	-1000×10^{-11}
InAs (approx)	$-10^7 \times 10^{-11}$

Table 3.1.Experimental Hall Coefficients obtained by conventional methods

A few words must also be said about the electrical conductivity σ. This may be defined by writing

$$j_x = \sigma E_x \tag{3.8}$$

and since $j=neV$, where V is the velocity and n is the concentration of electrons we obtain

$$\sigma = ne\frac{v_x}{E_x} \tag{3.9}$$

If Ohm's law is obeyed, as it normally is under the conditions we are concerned with, then σ must be independent of E so that (3.9) can be written

$$\sigma=ne\mu \tag{3.10}$$

μ is the electron drift velocity per unit electric field, or the mobility. This is a characteristic of the conductor and must be, within the validity of Ohm's law, independent of E. Equation (3.10) shows that σ depends upon two characteristics of the conductor: the density n of the charge carriers and their mobility μ. The interpretation of measurements of conductivity is therefore not so straightforward as that of the Hall effect, but the combination of the two yields that very informative quantity, the mobility. From the definition of the Hall coefficient and (3.10),

$$|R|\ \sigma=\mu \tag{3.11}$$

It is a convention to regard μ as a positive quantity regardless of the sign of R. The quantity defined by equation (3.11) is called the Hall mobility, while the mobility defined by equation (3.10) is called the conductivity mobility.

3.3. Measurement with Hall Sensors

One very important part of studying advanced materials is studying their magnetic properties. More specifically, we can learn a lot about a material by mapping its magnetic field as a function of position on the material's surface. One way of creating such a map is with scanning Hall probe microscopy. A Hall probe measures the magnitude of the perpendicular component of magnetic field at a point just above the surface of the material, then proceeds scanning across the material taking measurements until the map is created. As charge carriers move trough the magnetic field, they shift to one side of the two-dimensional wire, creating a bias potential across the other two leads, which is directly proportional to the average magnetic field across the active region.

Resistivity and Hall-coefficient measurements at different temperatures play an important part in research on semiconductors, such as germanium and silicon. From these quantities, the mobility and concentration of the charge carriers are found. Such measurements are commonly carried out with a test bar as in illustrated in Figure 3.1.
To determine the Hall coefficient the bar is subjected to a magnetic field applied at right angles to the direction of the current and to the line connecting to diametrically opposite contacts. From the potential difference produced between these latter contacts the Hall coefficient can be determined.

In measurements performed at low temperatures- e.g. in liquid nitrogen – point contacts possess resistances of the order of mega-ohms, in consequence of which the voltages can not be determined with sufficient accuracy. In such cases 'bridge shaped' samples are used. The voltage and current contacts here have a relatively large surface area, and hence the contact resistances are low. High current experiments on a single crystal bismuth sample at 77°K under an applied magnetic field have been done [9] and it was found that the I-V characteristics deviates from Ohm's law, and the Hall coefficient decreases with increasing current at sufficiently high currents.

3.3.1. Four Point Probe

The schematic hall sample of Fig.3.2 has a variety of practical implementations. One of these is the geometry shown in Figure 3.3.

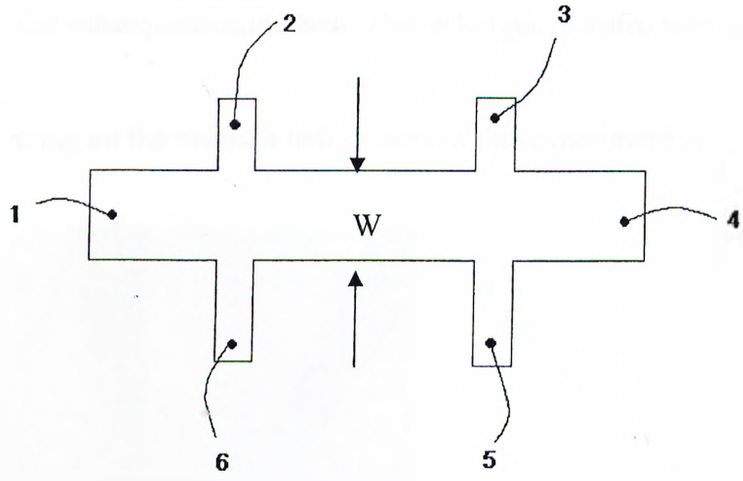

Fig.3.3. A bridge-type Hall Sample

This type of hall probe has four 'legs' for making the contacts and is known as a bridge-type Hall bar. The current flows into 1 and out of 4, the Hall voltage is measured between 2 and 3 or between 3 and 5 in the presence of a magnetic field. The resistivity is determined in the absence of the magnetic field by measuring between 2 and 3 or between 5 and 6. This structure allows not only the sheet resistance to be determined but the line width as well. The sheet resistance of such a bridge resistor is

$$\rho_s = \frac{W}{L}\frac{V_{23}}{I_{14}} \qquad (3.12)$$

The bridge structure is found to be sensitive to line-width variations of $\pm 0.1\mu m$ [10].

Conventional four-point measurements give an average resistivity. This is suitable for uniformly doped substrates but is not sufficient for non-uniformly doped samples in which resistivity *profiles* need to be determined.

Hall measurements are generally made on samples from which an average carrier concentration is derived. For uniformly doped samples the correct concentration is obtained but for non-uniformly doped samples the layers can be stripped reliably by anodic oxidation and subsequent oxide etch. The technique has also been applied to GaAs [11].

The numbering on the bismuth hall sensors in this experiment is shown in Fig. 3.4

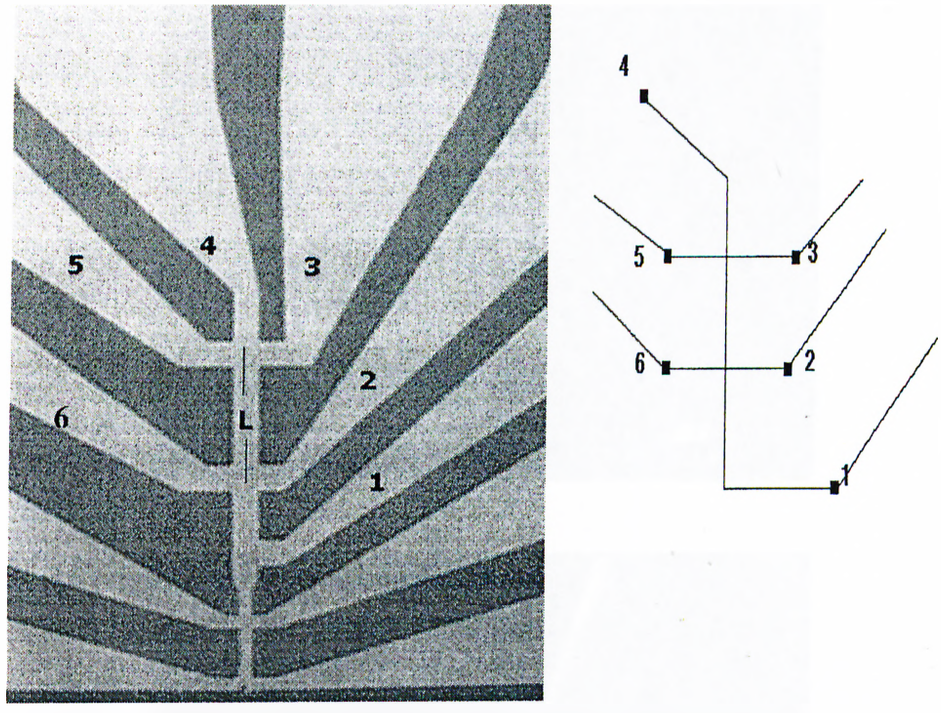

Figure 3.4. Electrical connections of Bismuth Hall sensor with L=50μm.

All the parts (from 1 to 6) are connected to the chip holder with gold wires. The technique is called 'bonding'. 3 wires are connected for each part to avoid from loosing contact since gold wires can be broken easily (Fig.3.5).

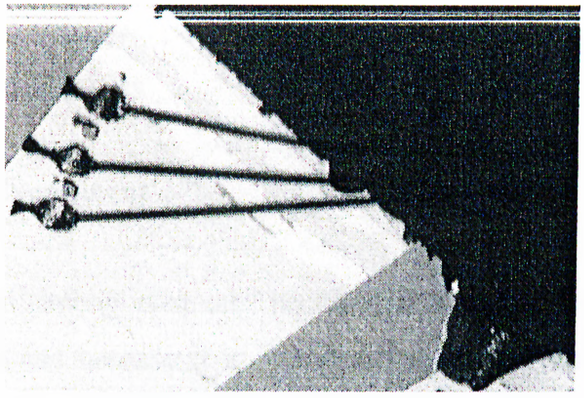

Figure 3.5. Bonding of Bi Hall sensors

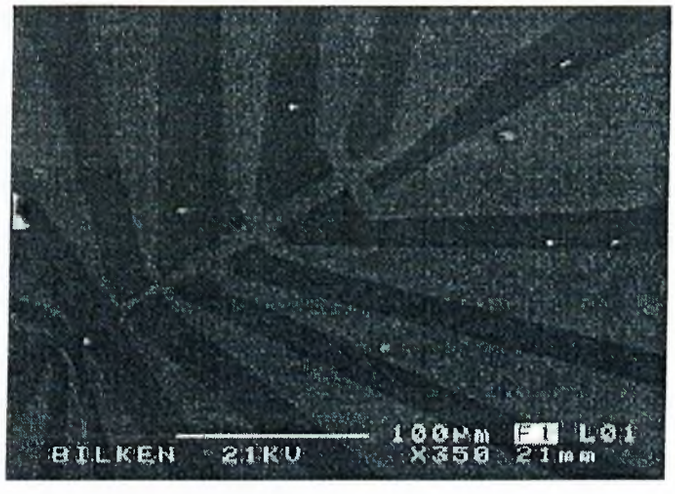

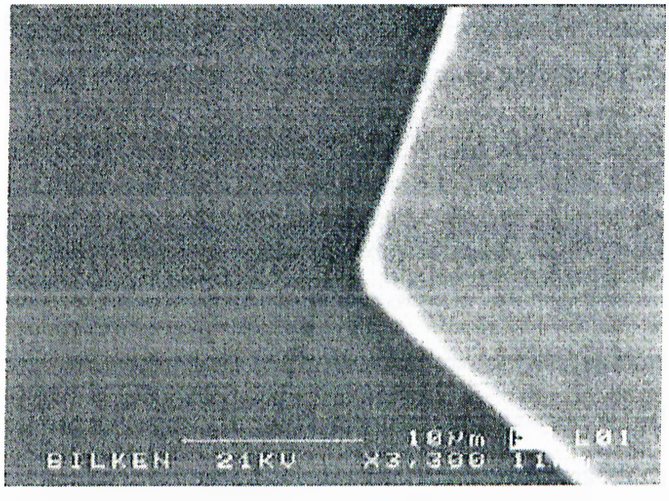

Figure 3.6. SEM images of Bismuth Hall Sensors

Chapter 4

Measurements and Results

4.1 Overview of the Experiment

Bismuth is unique among elements because of its low intrinsic carrier density compared with metals and because it is compensated (i.e., it has the same number of electrons as holes). Pure samples have less elastic scattering of the charge carriers and a longer scattering length compared with their impure counterparts.

Past studies of Bismuth [16-18] have concentrated on resistivity as a function of magnetic field at a given temperature, with particular attention paid to the Shubnikov-de Haas effect, i.e., the existence of magnetic-field-dependent oscillations in the resistivity at high magnetic fields and low temperatures. Bismuth reacts unusually to the presence of magnetic fields, exhibiting a change in resistance of 5 orders of magnitude at low temperatures in a field of 7 T [19]. This study, however focused primarily on measuring resistivity under no magnetic field at room temperature.

The measurements were computer-controlled, by Scanning Hall Probe Microscopy (SHPM 1.4.7) software. This enabled us to produce very weak current (of the order of microamper) to flow across the Hall probe. In the first part of the study, the resistivities of bismuth micro hall sensors with thickness 30 nm and 50 nm were measured under no magnetic field. For the Hall coefficient to be measured, a coil was designed to obtain the required magnetic field. The strength of the magnetic field at the center of the coil was calculated to have a coil constant of 17 Gauss/Volt. Calibration was performed with a Toshiba Hall probe whose Hall coefficient was previously known. The coil has a resistance of 33 Ω. The current was driven starting from ±500 μA ending at ±1000μA. Then the corresponding B-H curves were obtained with the number of averages set to 20 by the software. The electronics can supply ±10 V from the coil output of the DAC card. The Hall voltage (transverse, 3-5 or 6-2) is the potential difference

caused by accumulation of charge at sides of the semi-metal due to currents flowing in the presence of the magnetic field perpendicular to the longitudinal current (along 1-4).

4.1.1. Experimental Set Up and Calculations

The electronics system is composed of modules with different functions and the case. The electronics should be switched on before the software is switched on. The electronics included the following modules: Power supply, Micro A/D card, HP Amplifier card and the controller card. Power supply generates all the relevant regulated voltages (+220 V, -220 V, +15 V, -15 V, +8V, -8V, +450 V). Micro A/D card facilitates the computer interface using RS-232 serial port and PCI I/O card. It measures the relevant 8-channels of voltages with 16 bit resolution at a maximum speed of 200k sample/s. Controller card includes the external input which is used for reading any voltage value into the card and for AFM feedback. The hall current is generated and hall voltage is processed (amplified, shifted and filtered) by Hall Probe Amplifier card. The range of the hall current can be selected to be ± 100μA or ±1000 μA. Hall current outputs are I_{Hall} + and I_{Hall} -. The hall current can be switched on or off under software control. There is a x1001 gain Hall probe amplifier at the box attached to the head. Output of this amplifier is connected to V_{Hin} input of the HP AMP card. This input is amplified by the card and output to the front panel V_{Hout} for monitoring. The software can set post-amplifier gain as x1, 10, 100, 1000.

The experimental configuration used for measuring resistivity of thin Bismuth films is shown in Figure 4.1. Hall current was adjusted from –400 μA to +400 μA by 10 μA steps. Then the corresponding voltage was measured across the connections 5 and 6 or 2 and 3.

Results are given in Figure 4.2 for two Bismuth thin films having different thickness. The data for 30 nm thick Bismuth film were found to satisfy the following equation:

$$V_{56}=0.3772 \times I_{Hall} + 7.8444$$

Using the equation (3.12) and knowing the fact that L=50 μm and W=10 μm ,the sheet resistance is calculated to be ρ_S= 75 Ω/□.

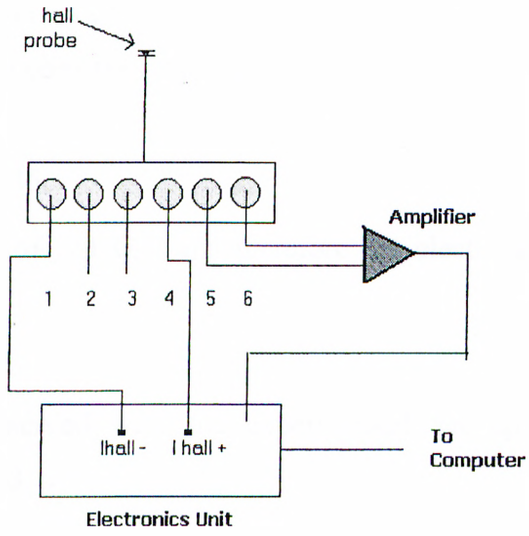

Figure 4.1. Experimental configuration used to measure the resistivity.

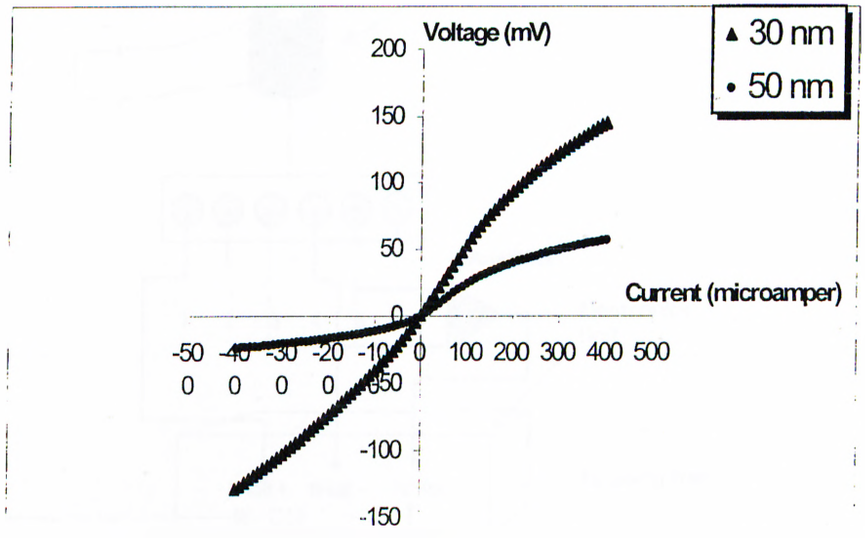

Figure 4.2. Hall current versus voltage across connections 5 and 6.

For the bismuth film whose thickness is 50 nm, the slope of the I-V curve yields the electrical resistivity of $22.6 \times 10^{-5}\ \Omega$ cm.

The voltage measurement across connections 6-2 versus hall current for the 50 nm thick bismuth film was observed to obey the relation,

$$V_{56}=0.1191 \times I_{Hall} + 10.535$$

This results in a sheet resistance of 23 Ω/□ and therefore the electrical resistivity of $1.2\times 10^{-5}\ \Omega$ cm.

The Hall effect was observed with the experimental set up whose main components are shown in Figure 4.3.

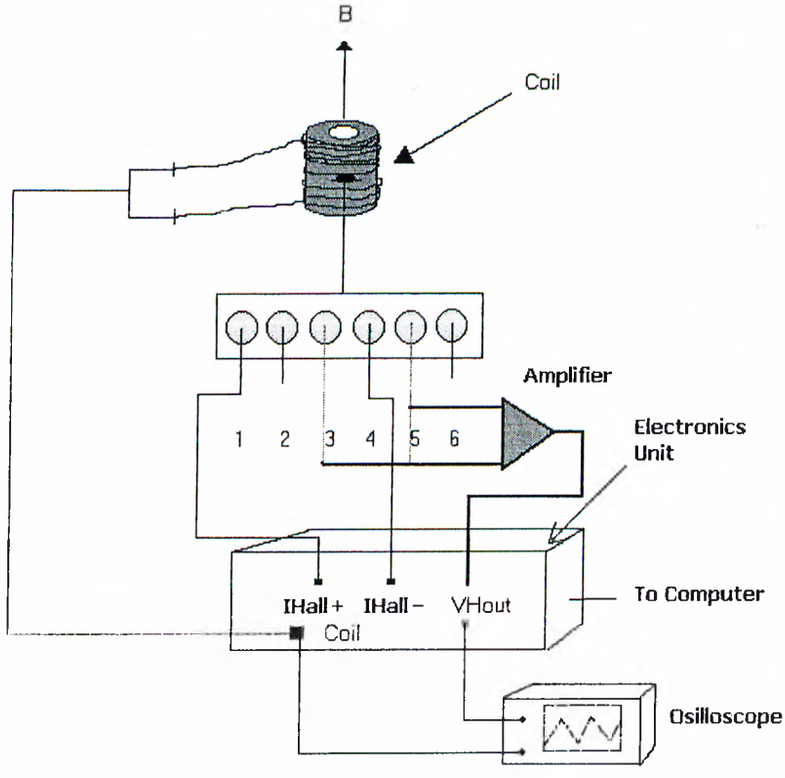

Figure 4.3. Main components of the Hall effect experiment.

The system was designed for operation at room temperature. Magnetic field was generated by the coil that was sent $\pm$ 10 V by the DAC card of the electronics. This enabled us to obtain magnetic field oscillating between $\approx \pm$ 200 Oe. The corresponding B-H curves were shown below. The slope was calculated for each B-H curve from which the Hall coefficient of the thin Bismuth films was estimated. The sign of the Hall coefficient was maintained due to the SHPM 1.4.7. Software even when the direction of the current was changed. Initially, the Hall coefficient was set to one in the options menu of the software then the corresponding slope of B-H curve was obtained. At the calibration of the coil, for instance, when the previously known Hall coefficient was given, the slope of the B-H curve was obtained to be one as expected supposing the experimental configuration was correctly set up.

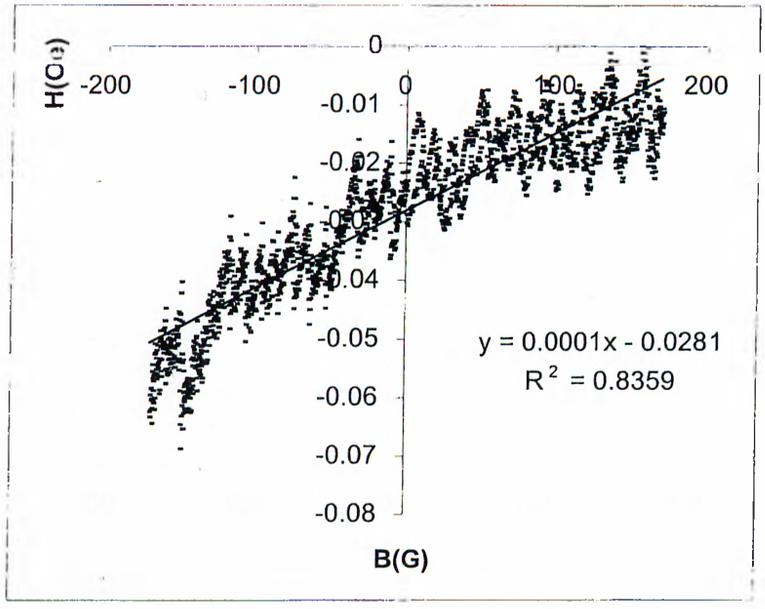

Figure 4.4. B-H curve of 30 nm thick Bi film. I_{Hall}= +500 μA.

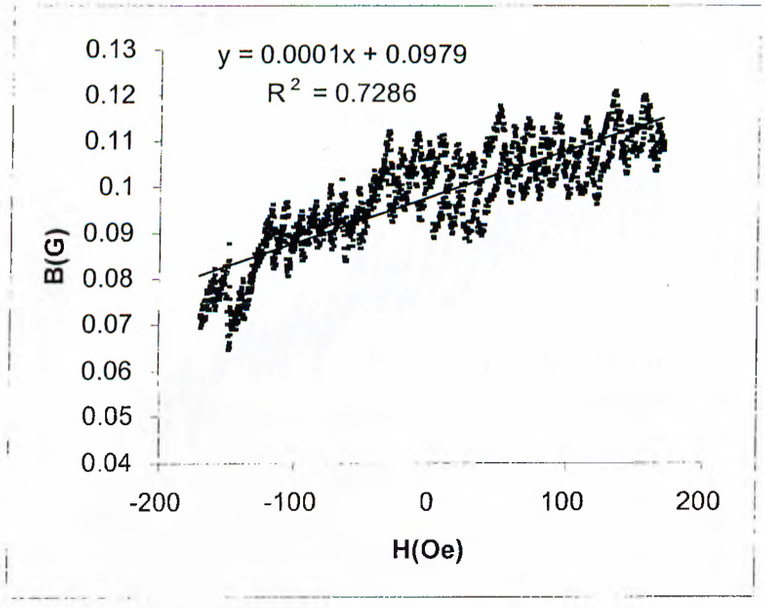

Figure 4.5. B-H curve of 30 nm thick Bi film. I_{Hall} = +600 μA.

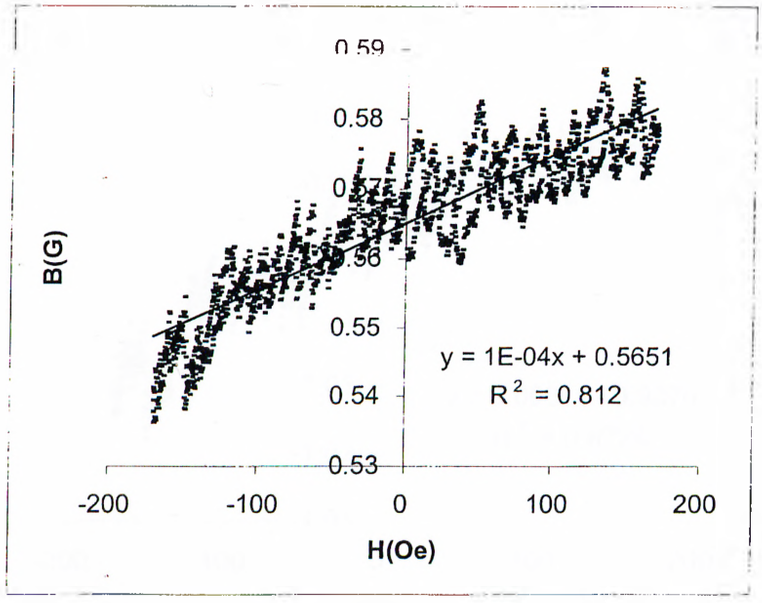

Figure 4.6. B-H curve of 30 nm thick Bi film. I_{Hall} = +700 μA.

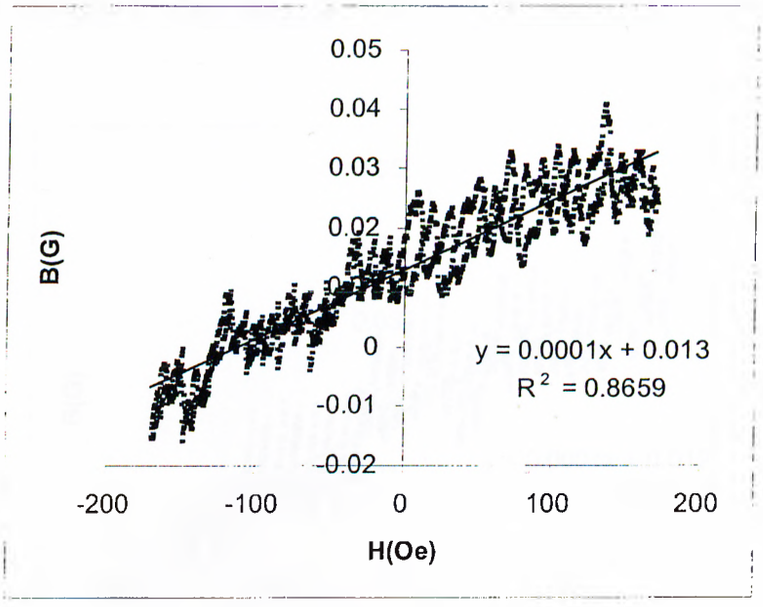

Figure 4.7. B-H curve of 30 nm thick Bi film. I_{Hall} = +800 μA.

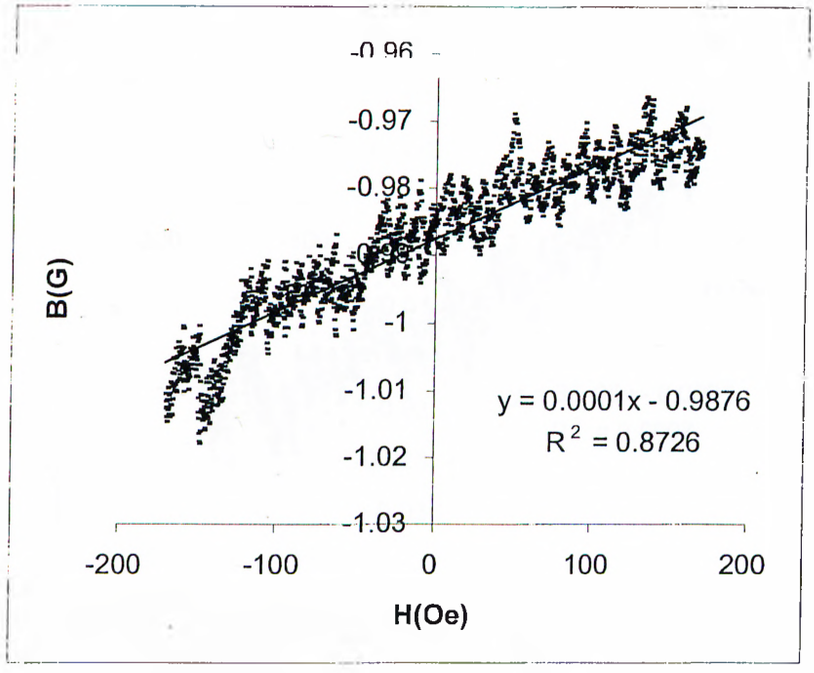

Figure 4.8. B-H curve of 30 nm thick Bi film. I_{Hall} = +900 μA.

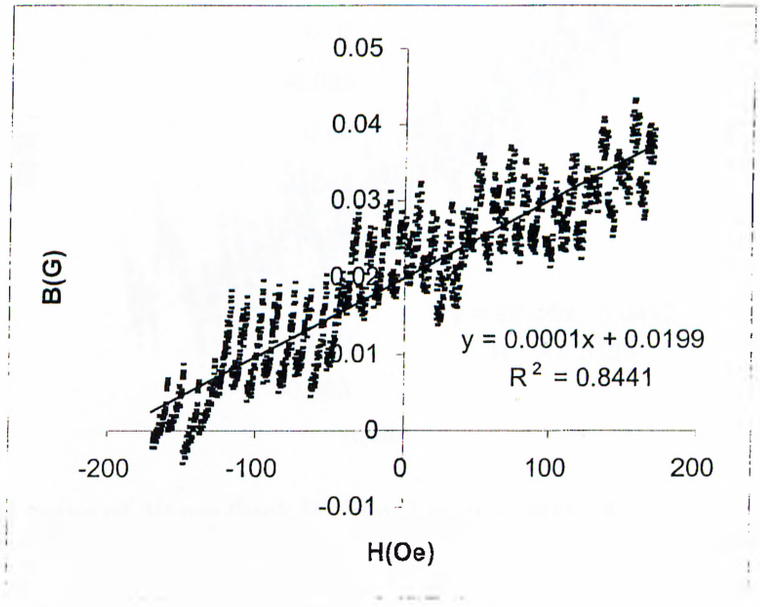

Figure 4.9. B-H curve of 30 nm thick Bi film. I_{Hall} = +1000 μA.

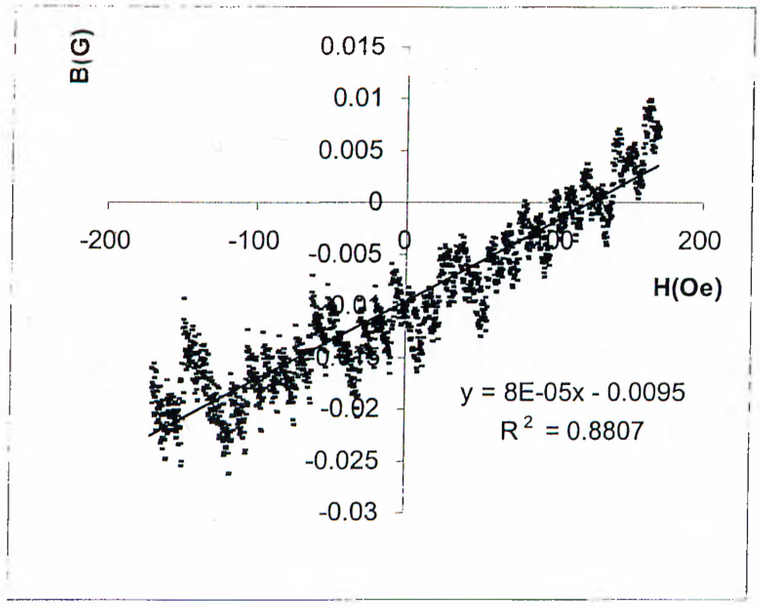

Figure 4.10. B-H curve of 30 nm thick Bi film. I_{Hall} = -1000 μA.

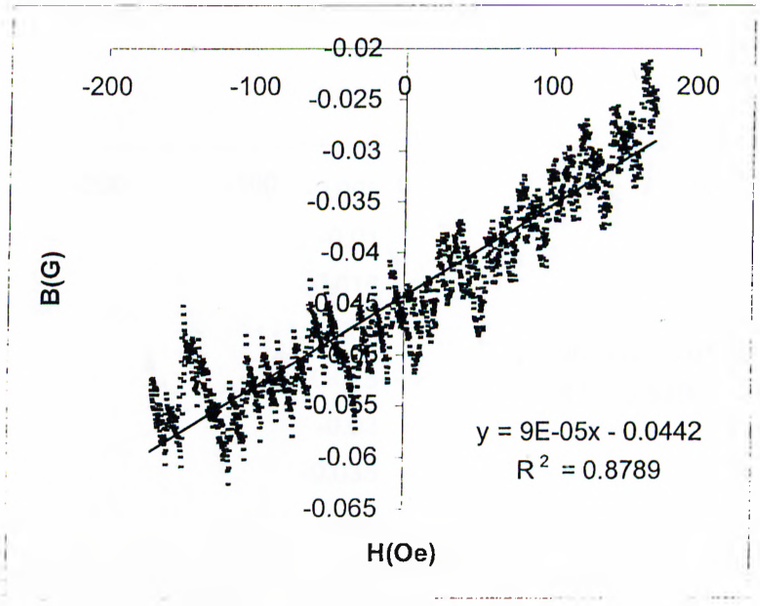

Figure 4.11. B-H curve of 30 nm thick Bi film. I_{Hall} = -900 μA.

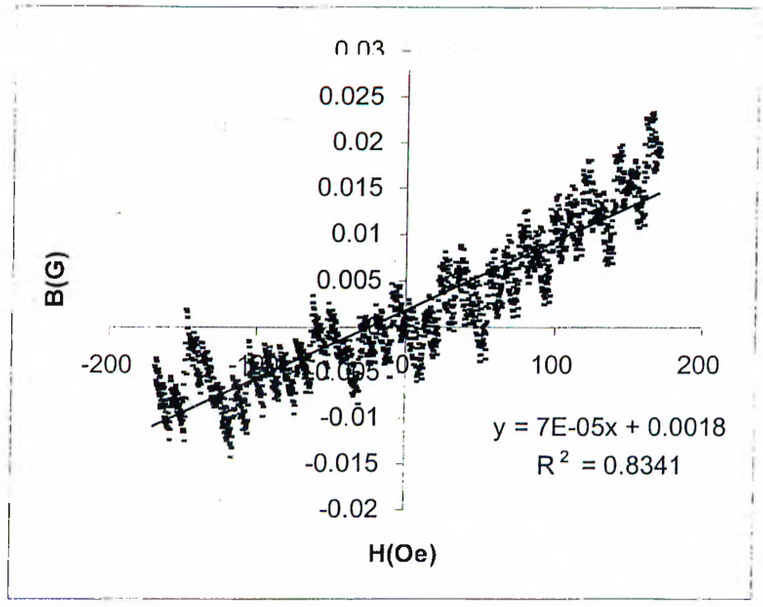

Figure 4.12. B-H curve of 30 nm thick Bi film. I_{Hall} = -800 μA.

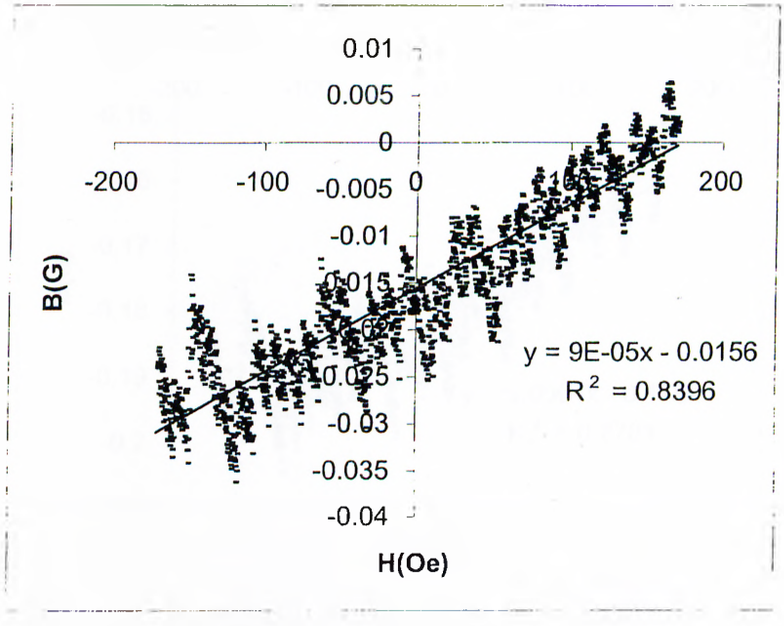

Figure 4.13. B-H curve of 30 nm thick Bi film. I_{Hall} = -700 μA.

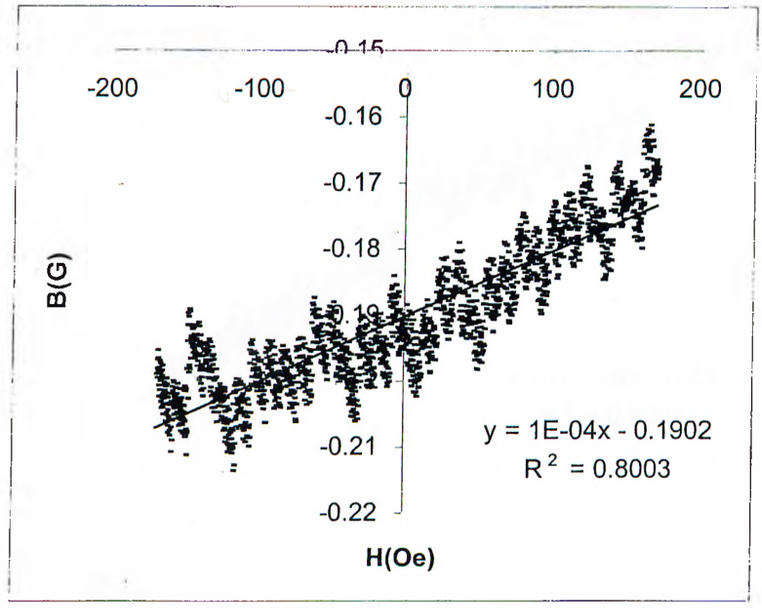

Figure 4.14. B-H curve of 30 nm thick Bi film. I_{Hall} = -600 μA.

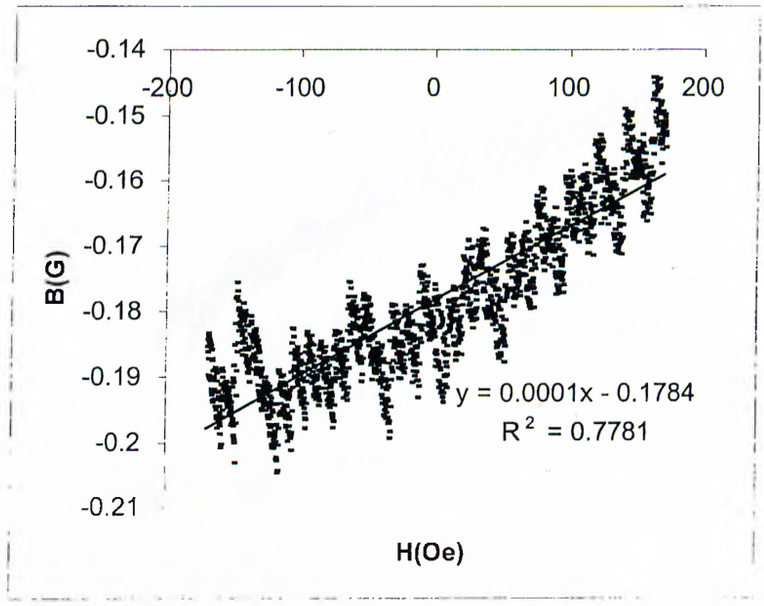

Figure 4.15. B-H curve of 30 nm thick Bi film. I_{Hall} = -500 μA.

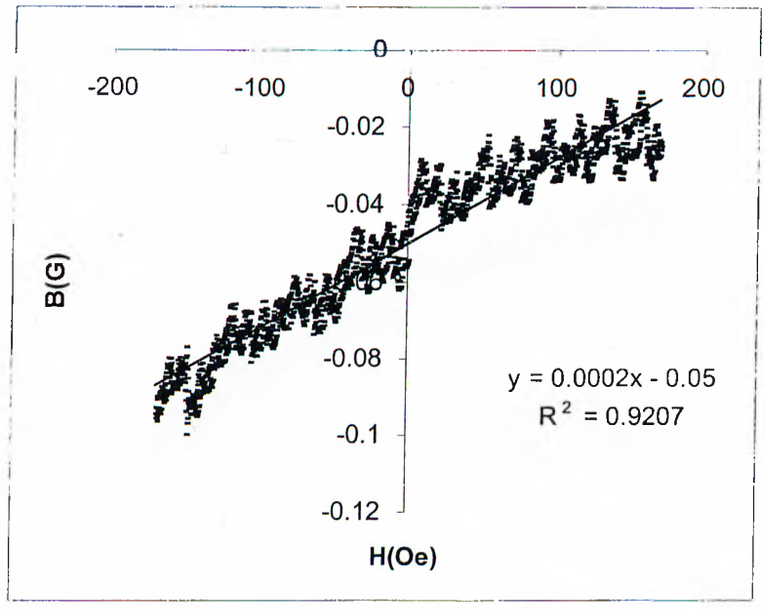

Figure 4.16. B-H curve of 50 nm thick Bi film. I_{Hall} = +500 μA.

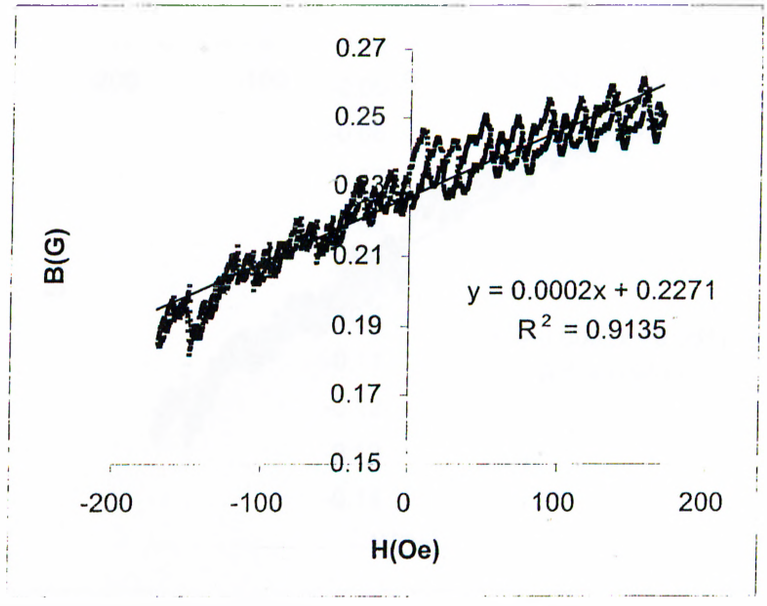

Figure 4.17. B-H curve of 50 nm thick Bi film. I_{Hall} = +600 μA.

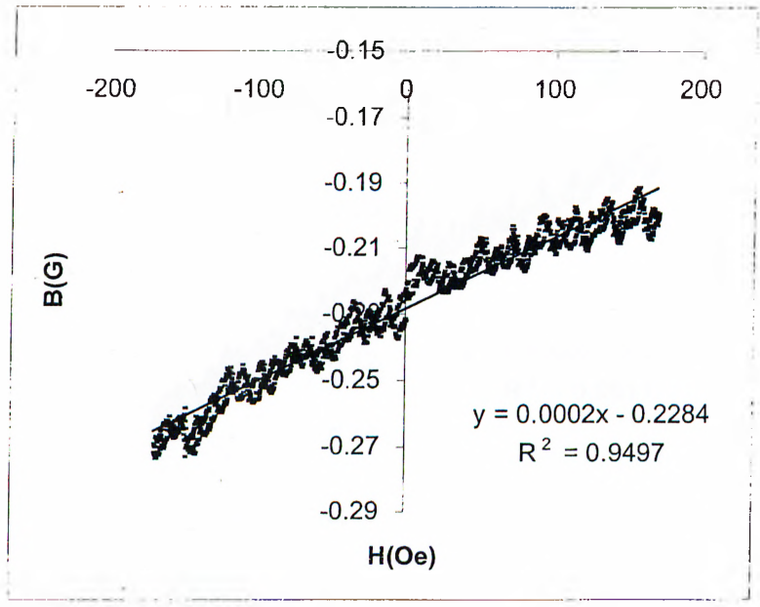

Figure 4.18. B-H curve of 50 nm thick Bi film. I_{Hall} = +700 μA.

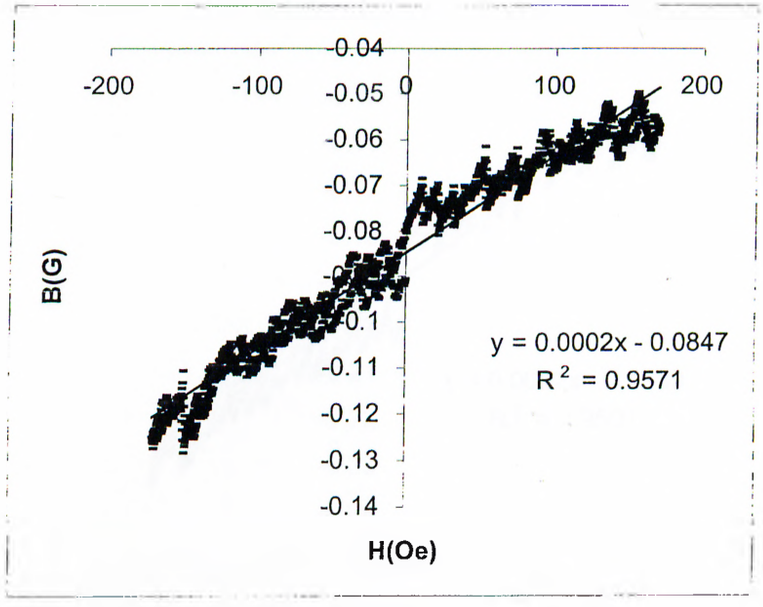

Figure 4.19. B-H curve of 50 nm thick Bi film I_{Hall} = +800 μA.

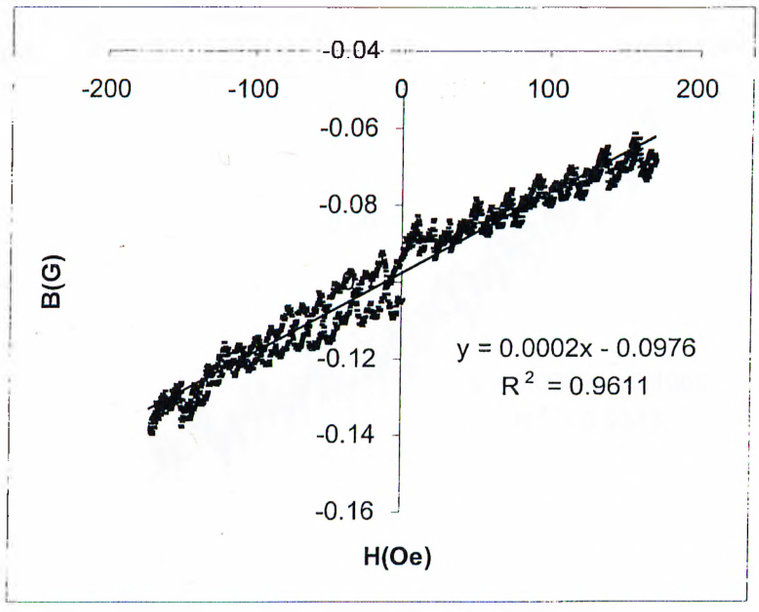

Figure 4.20. B-H curve of 50 nm thick Bi film. I_{Hall} = +900 μA.

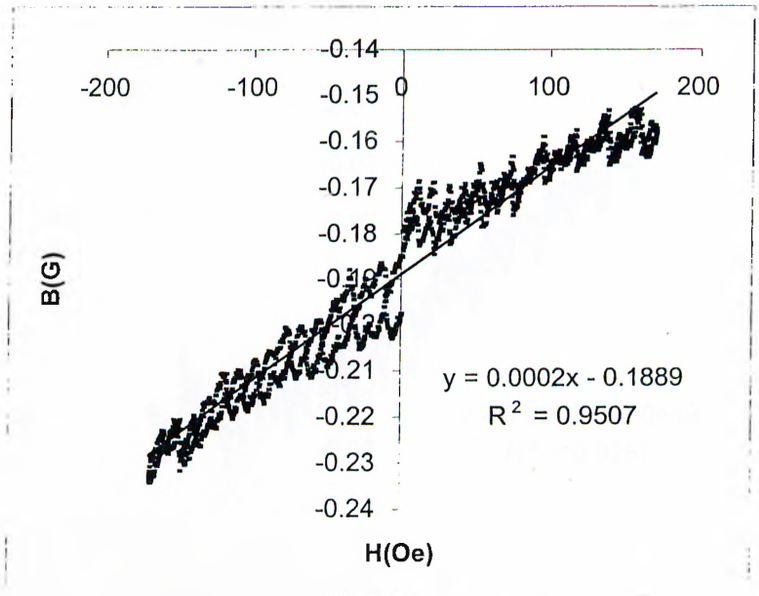

Figure 4.21. B-H curve of 50 nm thick Bi film. I_{Hall} = +1000 μA.

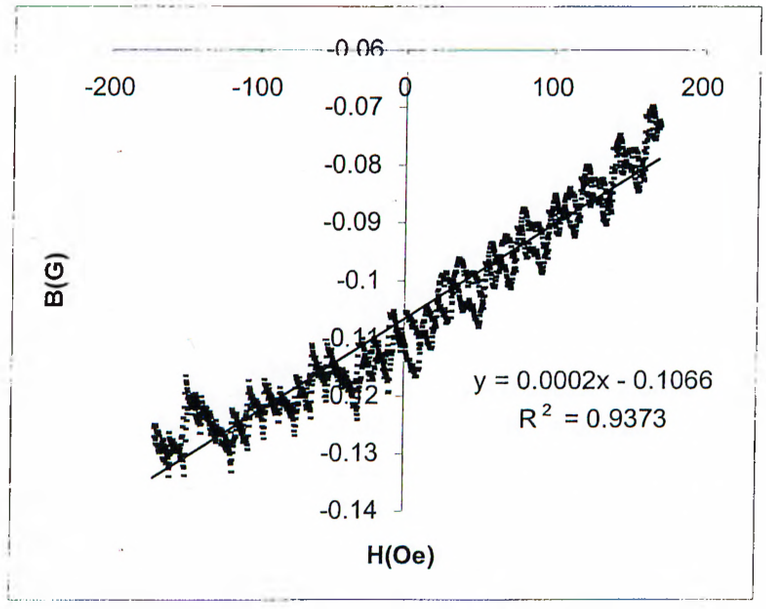

Figure 4.22. B-H curve of 50 nm thick Bi film. I_{Hall} = -1000 μA.

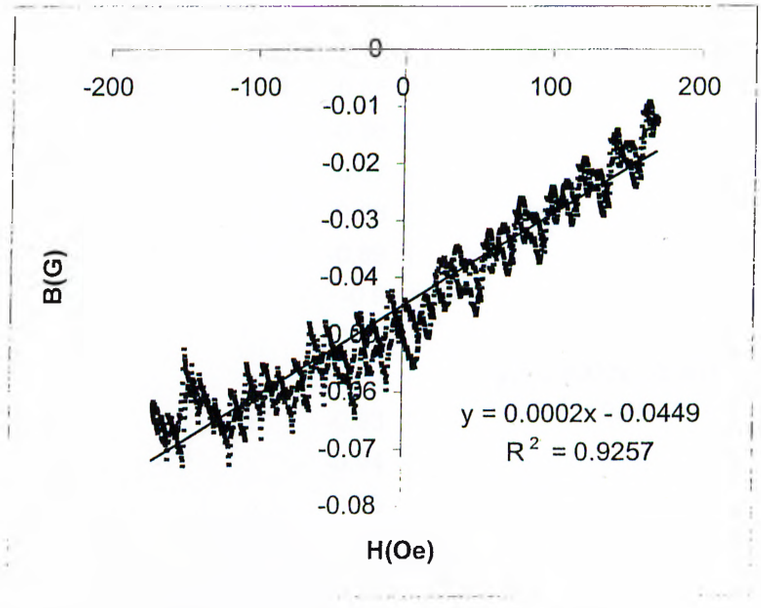

Figure 4.23. B-H curve of 50 nm thick Bi film. I_{Hall} = -900 μA.

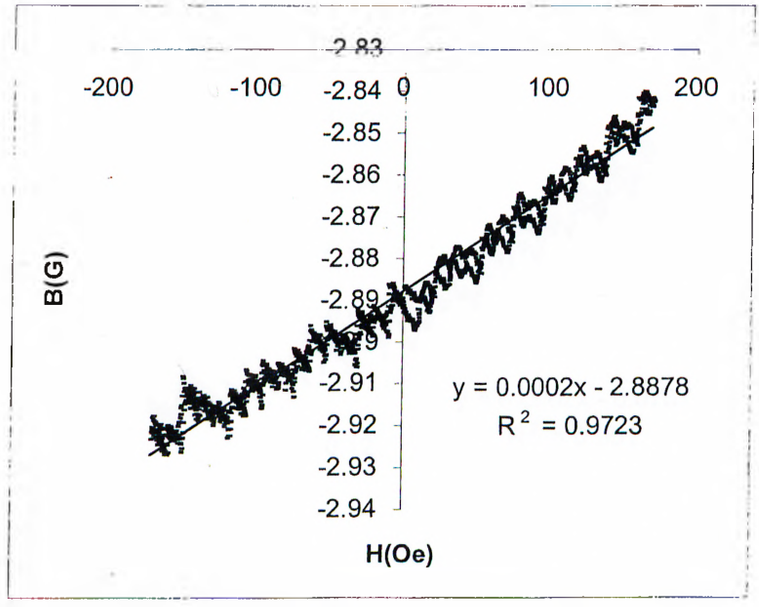

Figure 4.24. B-H curve of 50 nm thick Bi film. I_{Hall} = -800 μA.

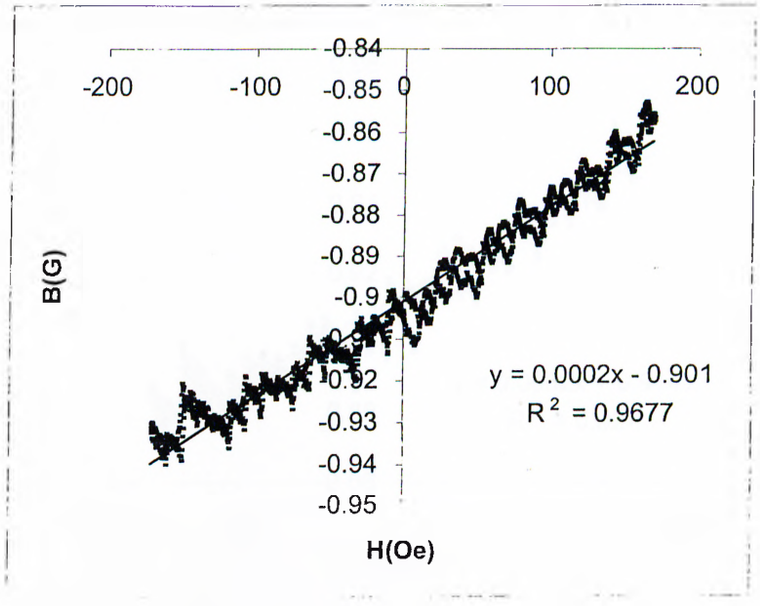

Figure 4.25. B-H curve of 50 nm thick Bi film. I_{Hall} = -700 μA.

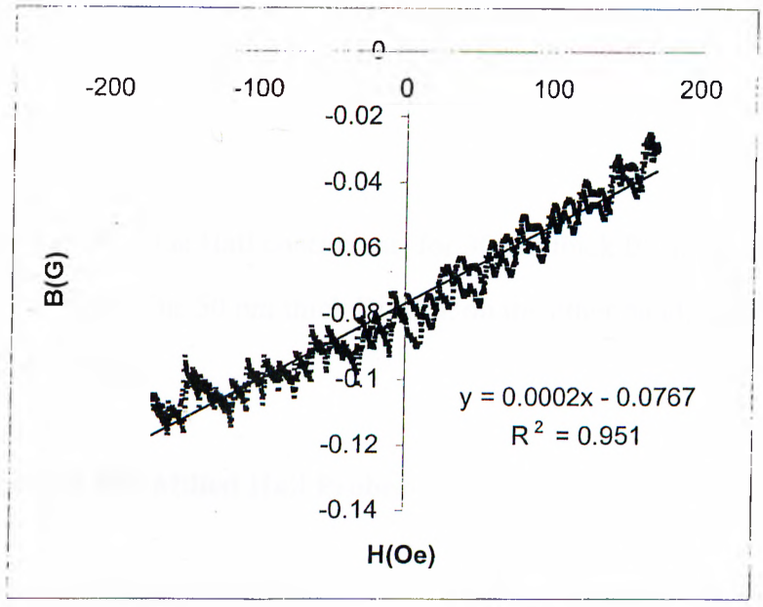

Figure 4.26. B-H curve of 50 nm thick Bi film. I_{Hall} = -600 μA.

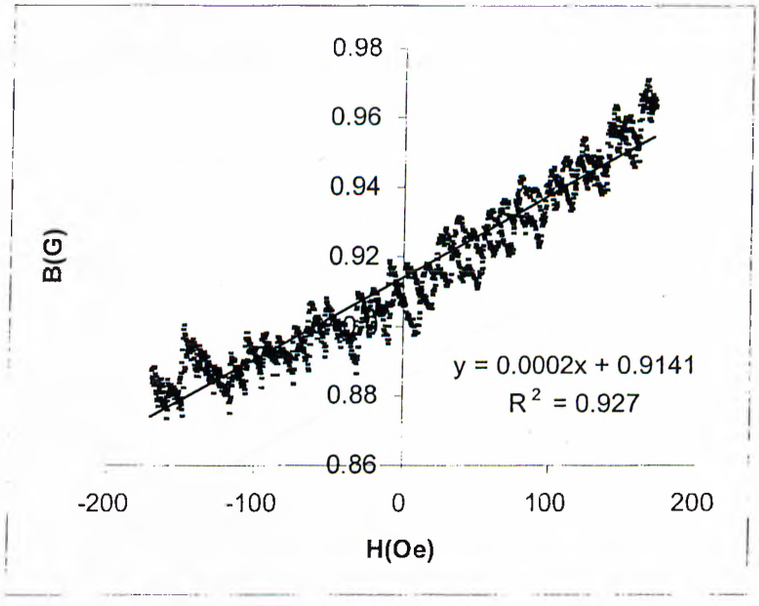

Figure 4.27. B-H curve of 50 nm thick Bi film. I_{Hall} = -500 μA.

The Hall amplifier gain was set to 1 in the B-H curve measurements for convenience. The Hall voltage measured at the output of the low noise amplifier is a function of

applied Hall current (I hall), gain of the amplifier (G), the Hall coefficient (R_H) and the magnetic field (B) perpendicular to the sensor.

$$V_H = I_{Hall} \times R_H \times B \times G \qquad (4.1)$$

The slope of the B-H curve (the Hall coefficient) for 30 nm thick Bi film varies between 7×10^{-5} and 1×10^{-4} Ω/G. The 50 nm thick Bi film, on the other hand, gives a Hall coefficient of 2×10^{-4} Ω/G.

4.2. Measurements of FIB-Milled Hall Probes

The similar measurements were done by Prof. Adarsh Sandhu* for Bi-nano Hall sensors of ≈0.25 μm × 0.25 μm size, and the Hall coefficient was calculated. The hall voltage versus hall current at H_{ext} = 1483 Oe. was pictured in Figure 4.28. B-H curve of the probe was depicted in Figure 4.29.

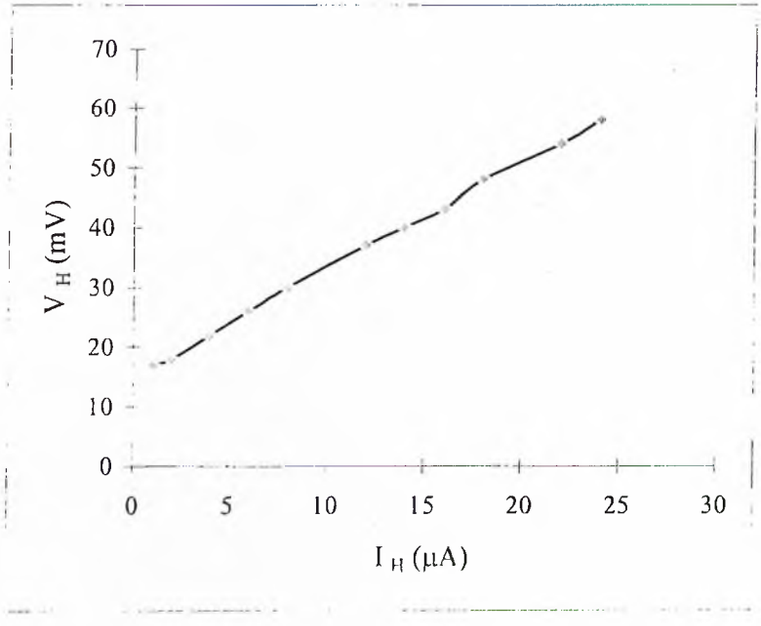

Figure 4.28. I-V characteristic of Bi-nano Hall probe milled by FIB, H=1483 Oe.

* Department of Electrical and Electronic Engineering, Tokai University, sandhu@keyaki.cc.u-tokai.ac.jp

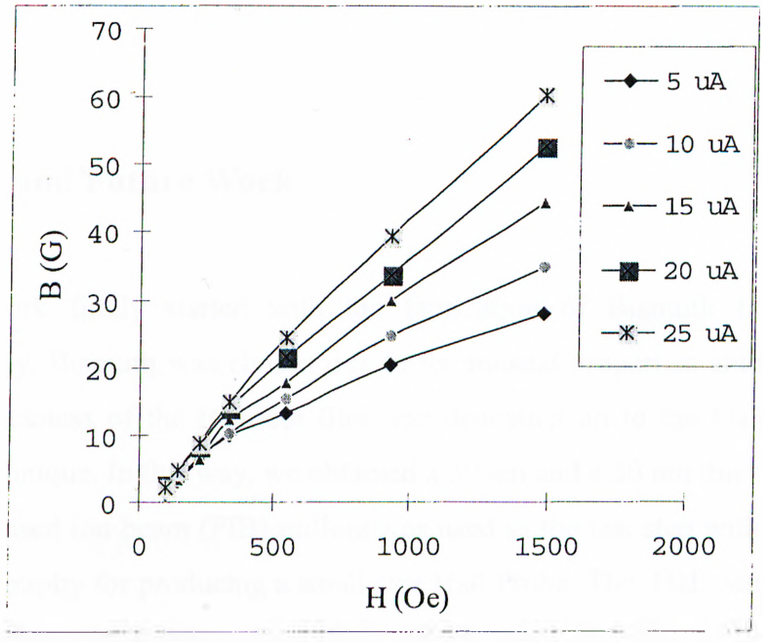

Figure 4.29. B-H curve of Bi-nano Hall probe milled by FIB

Chapter 5

Conclusions and Future Work

This work firstly started with the fabrication of Bismuth Hall sensors by photolithography. Bismuth was chosen due to its unusual properties among other semi-metals. The thickness of the Bismuth film was deposited on to the GaAs substrate by evaporation technique. In this way, we obtained a 30 nm and a 50 nm thick film.

The focused ion beam (FIB) milling was used as the last step with a combination of optical lithography for producing a small size Hall Probe. The Hall coefficient for this probe was calculated to be $R_H = 2.1 \times 10^{-4}$ ohm/G by Prof. A. Sandhu.

The measurement part consisted mainly of two parts one of which was the resistivity measurement. The resistivity of the Bismuth hall sensor was found to be 22.5×10^{-5} Ω cm for 30 nm Bi film and 1.2×10^{-5} Ω cm for 50 nm Bi film which are in good agreement with [20]. [22] states that at room temperature, the resistivity is mainly determined by the intrinsic property of the Bi films and hence all samples show essentially the same resistivity. This is mainly obeyed in our study.

The second part focused on the determination of the Hall coeffient which is a very important quantity since important facts about how metals and semiconductors behave can be concluded after determination of this constant. In the experiment of Hall effect, it was seen that the Hall coefficient was found to have a positive value even when the direction of the current was changed. The 30 nm and 50 nm Bi films were found to have a hall coefficient of $\sim 1 \times 10^{-4}$ Ω/G and 2×10^{-4} Ω/G respectively which are again in good agreement with [21].

There, however, can be some factors that have an influence on our results, like the noise sources coming from the electronics, the noise coming from the intrinsic properties of the probe itself, the lithographic character of the probe and maybe some environmental

effects; there can be air contamination. For this reason, the hall probes were kept inside a vacuum system when they were not in use.

As a future work, such measurements can also be performed under different temperature values, initially at 77K. The strength of the magnetic field can also be changed as another parameter, since Bismuth is a magnoresistance. In addition, Bismuth is a promising alternative for magnetic imaging; the use of Bi for fabricating Hall probes is an important advance for room temperature magnetic imaging of ferromagnetic surfaces on the nanometer scale. The thickness dependence of the resistivity, Hall coefficient and the magnetoresistance coefficient can also be investigated. The variation of the Fermi energy becomes very important in understanding the temperature dependence of the transport phenomena, in particular at low temperatures.

Bibliography

[1] PM. Vereecken, L. Sun, PC. Searson, *Magnetotransport properties of bismuth films on p-GaAs,* J.Appl. Phys. **88**, 6529 (2000)

[2] S. Cho, Y. Kim, A.J. Freeman, J.Appl. Phys. Lett. **79**, 3651 (2001)

[3] Yu.F. Ogrin et al, Pis'ma Zh. Eksp. Teo. Fiz. **3**,114 (1966)

[4] C. A. Hoffman, J.R.Meyer, *Semimetal-to-semiconductor transition in bismuth thin films,* Phy. Rev. B **48**, 11431 (1993)

[5] Microchip Fabrication, P. V. Zant, 2nd Edition, chapter 8, 9, 13 Mac-Graw-Hill Comp. (1990)

[6] AIP handbook, 3rd Edition, Dwight E. Gray, New York (1972)

[7] Metals Handbook, 8th Edition, vol.1, T.Lyman, OH (1961)

[8] Introduction to Solid State Physics, C. Kittel, 4th Edition, John Wiley&Sons, (1971)

[9] S. Tosima, R.Hirota, *Effect of the Self-Magnetic Field on Galvanometric Effects in Bismuth*, Laboratories RCA Inc., Tokyo, IBM Journal, July (1964).

[10] M.G. Buehler, S.D. Grant, J. Electrochem. Soc. **125**, 650 (1978)

[11] H. Müller, F.H. Eisen, J. Electrochem. Soc. **122**, 651 (1975)

[12] N. Garcia, Y. H. Kao, *Galvanometric Studies of Bismuth Films in the Quantum-Size-Effect Region,* Phys. Rev. B, **5**, 2029 (1972)

[13] Yu. F. Kommik *et al.*, Zh. Eksp. Teo. Fiz. **60**,669 (1971)

[14] V.N. Lutskii, Pis'ma Zh. Eksp. Teo. Fiz. **2**,391 (1965)

[15] V.B. Sandomirskii, Zh. Eksp. Teo. Fiz. **52**,158 (1967)

[16] Y. Iye, L. E. McNeal, Phys. Rev. **135**,1118 (1964)

[17] R. D. Brown III, Phys. Rev. B **2**,928 (1970)

[18] E. M. Lifshitz and L.P. Pitaevskii, *Physical Kinetics,* (Nauka, Moskow,1979)

[19] Special Report : REU Program, A. F. Hebard, J. Derakhshan, University of Florida

[20] G. T. Meaden, *Electrical resistance of metals*, Plenum (1965).

[21] A. Sandhu, H. Masuda, K. Kurosawa, A. Oral, Elect. Lett, **37**, 1335 (2001)

[22] F. Y. Yang, P. C. Searson, *Large Magnetoresistance and finite size effect in electrodeposited bismuth lines*, J. Appl. Phys, **89**, 7206 (2001).

[23] M.R Black, M. Padi, *Intersubband transitions in bismuth nanowires*, J.Appl. Phys. Lett. **77**, 4142 (2000)

[24] Focused Ion Beam Technology and Applications, Steckl, A. J., in Emerging Technologies for in-Situ Processing, NATO ASI series, M. Nijhoff Publishers, pp.179-199 (1988)

[25] Xu Du, A.F. Hebard, *Large Magnetoresistance of Bismuth/gold films thermally deposited onto glass substrates*, J.Appl. Phys. Lett. **82**, 2293 (2003)

[26] A. Sandhu, H. Masuda, A. Oral, *Room Temperature scanning Hall Probe Microscopy using GaAs/AlGaAs and Bi micro-Hall Probes*, Ultramicroscopy, **91**, 97 (2002)

[27] G. Jung, M. Ocio, J.Appl. Phys. Lett. **78**, 359 (2001)

[28] J. A. van Hulst, H. M. Jaeger, Phys. Rev. B. **52**, 5953 (1995)

[29] A. Sandhu, H. Masuda, A. Oral , *Direct magnetic imaging of ferromagnetic domain structures by room temperature scanning Hall probe microscopy using a bismuth micro-hall probe,* Jpn. J. Appl. Phys. **40**, L524 (2001)

[30] A. Sandhu, H. Masuda, A. Oral, Proceedings of the Eighth International Conference on Ferrites, Kyoto, September 18-21 (2000)

[31] D. K. Schroder, *Semiconductor Material and Device Characterization*, pages 12, 73-77, 196-198, John Wiley & Sons (1990)

[32] Project no: 3, course PH3480, *Hall Effect Experiments with Metals and Semiconductors,* Michigan Technological University, Department of Physics.

[33] C. A. Hoffman, J.R.Meyer, *Reply to Semimetal-to-semiconductor transition in bismuth thin films,* Phy. Rev. B **51**, 5535 (1995)